P-Q CAPABILITY ANALYSIS OF INVERTER BASED RESOURCES WITH TYPICAL GRID CONNECTED FILTERS

by

BING LU

SHUHUI LI, COMMITTEE CHAIR

FEI HU
JINWEI SHEN

A THESIS

Submitted in partial fulfillment of the requirements
for the degree of Master of Science
in the Department of Electrical and Computer Engineering
in the Graduate School of
The University of Alabama

TUSCALOOSA, ALABAMA

2021

ABSTRACT

Traditionally, a P-Q Capability Chart is usually used to specify the safe operation boundary for a synchronous generator. With the increased development of inverter-based resources (IBRs) and interconnection of IBRs to the grid, IBR P-Q Capability Charts are also developed and proposed by the power industry to assure IBR operation efficiency and reliability. This thesis presents an evaluation about IBR control relation with the IBR P-Q capability, development of the IBR output active and reactive power models for IBR control in dq vector framework considering different filtering mechanisms and development of algorithms for computing IBR P-Q capability considering constraints that are specific to an IBR inverter and different from those for a synchronous generator. The proposed study considers the impact of different IBR grid-connected filters, IBR vector control implementation in the dq reference frame, and different pulse-width modulation methods applied to IBR inverters. The models and algorithms developed for the P-Q capability analysis have considered distinct IBR constraints that are different from those for a traditional synchronous generator. Also, this thesis presents a comprehensive evaluation of IBR P-Q capability curves under different conditions and P-Q capability theoretical evaluation for L-filter IBR. Both theoretical study for a special case and complete simulation evaluation are conducted to obtain IBR P-Q capability characteristics that are important for IBR control, operation and management, and for the development of international standards for interconnecting IBRs to the transmission and sub-transmission grids, such as IEEE P2800. In addition, this thesis present and derivate the equation for IBR P-Q

capability curve with L-filter, that can work in most different perimeters to help the IBR P-Q capability curve can work in different condition in industry.

DEDICATION

This thesis is dedicated to everyone who helped me and guided me through the process of creating this document.

LIST OF ABBREVIATIONS AND SYMBOLS

AC	Alternative Current
BPS	Bulk Power System
DC	Direct Current
DER	Distributed Energy Resource
DFIG	Doubly-Fed Induction Generator
EMT	Electromagnetic Transients
IBR	Inverter-Based Resource
PCC	Point of Common Coupling
PI	Proportional Integral
PMSG	Permanent Magnet Synchronous Generator
PV	Photovoltaic
PWM	Pulse Width Modulation
RIC	Rated Current Circle
SPWM	Sinusoidal Pulse Width Modulation
SVPWM	Space Vector Pulse Width Modulation

ACKNOWLEDGMENTS

Firstly, I would like to express my sincere gratitude to my advisor Dr. Shuhui Li for the continuous support of my research, for his patience, motivation, and immense knowledge. His guidance helped me in all the time of research and writing of this thesis. I could not have imagined having a better advisor and mentor.

Besides my advisor, I would like to thank the rest of my thesis committee: Dr. Fei Hu and Dr. Jingwei Shen, for their insightful comments and encouragement.

CONTENTS

LIST OF TABLES

LIST OF FIGURES

1. INTRODUCTION

1.1 Background

With the development of the electric grids and the increasing power generation from renewable resource, the renewable resources such as wind and solar photovoltaic (PV) power plants are become more and more important for the power system in United States and around the world. The renewable resources are 19.3% of humans' global energy consumption and 24.5% generation of electricity in 2015 and 2016. The globe investments in renewable energy is more than 286 billion [1]. The renewable resources are either completely or partially interconnected to the grid through power electronic inverters, hence referred to as inverter-based resources (IBRs). Although IBRs can present new opportunities in supporting grid control and responding to abnormal grid conditions, maintaining control effectiveness and reliability of an IBR presents a great challenge to the energy industry.

Traditionally, for a synchronous generator, a boundary within which the machine can operate safely is defined via the P-Q Capability Curve and is used to guide the control of the generator. It is also known as Operating Charts or Capability Charts [2, 3]. The permissible region of operation is restricted to the points as follows [4]: 1) The MVA rating of the generator should not be exceeded. This limit is determined by the heating of the stator windings caused by the armature current; 2) The MW loading of the generator should not go beyond the rating of the prime mover; 3) The field current should not exceed a rated value determined by the heating of

the field winding; 4) The load angle δ must be less than 90 degrees to assure the stable operation of the generator.

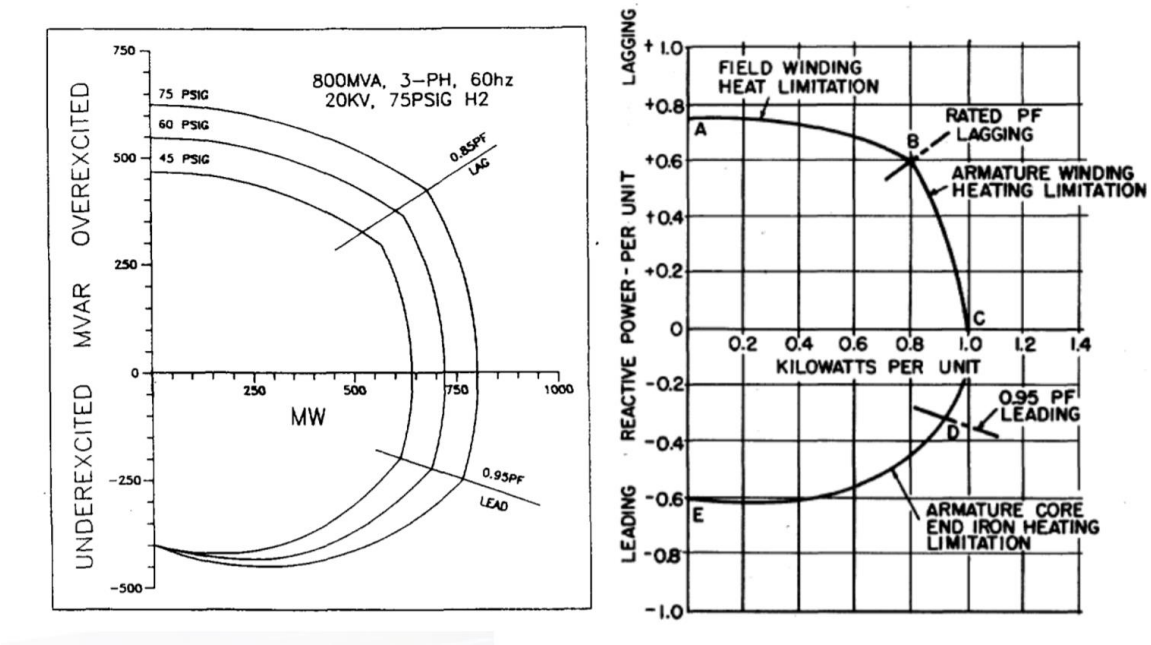

Fig. 1.1 Traditional Operating charts and Capability charts from [2, 3]

Similarly, to assure the safe operation of IBRs as well as the development of international standards for IBR grid interconnection, P-Q capability curves have also been proposed or developed in the power and electric utility industry. The NERC (North America Electric Reliability Corporation) Reliability Guideline in [5] presented an IBR capability curve with near semi-circle capability and another semi-circle IBR capability curve with fixed reactive capability at around 0.95 per unit active power output levels, both of which show reactive capability for nominal voltage, similar to a synchronous generator capability curve in Fig. 1.1. The Electric Reliability Council of Texas (ERCOT) presented a rectangle P-Q capability curve that needs to meet at the Point of Interconnection (POI) [6]. The Sandia's report about Reactive

Power Interconnection Requirements for PV and Wind Plants [6] presented triangular, rectangular and D-shape capability curves at the nominal voltage.

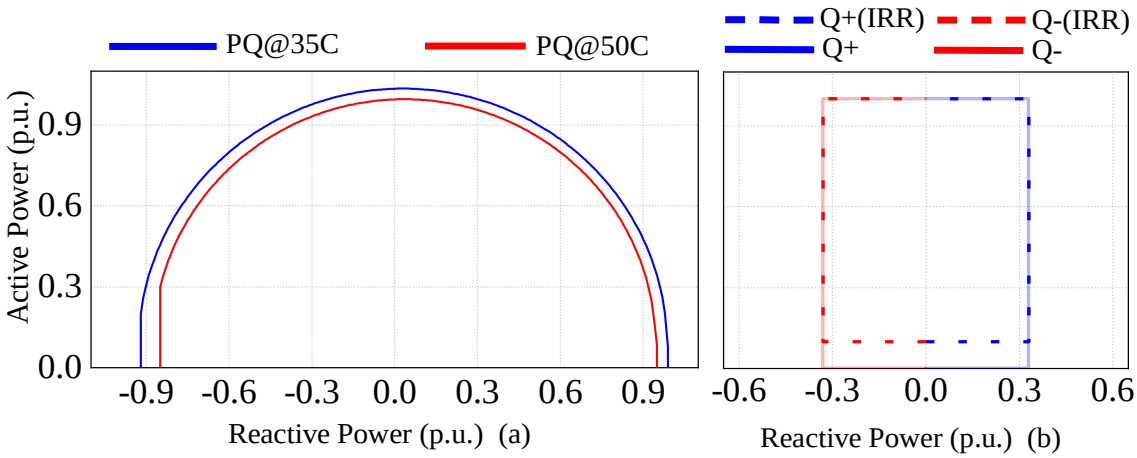

Fig. 1.2 IBR PQ capability curves from NERC [4] and ERCOT [5]

With the increasing penetration of inverter-based resources connected to the the bulk power system (BPS), the industry is faced with interconnecting new technologies with new capabilities as well as a rapidly changing landscape. Unlike synchronous generators that predominantly respond to grid events with classical mechanics, inverter-based resource response is driven by advanced controls. These controls are configurable and capable of providing similar essential reliability services (ERSs) as synchronous generating resources; however, the industry is faced with providing sufficient guidance during the interconnection process to clearly describe what capabilities and control settings are desired. Due to the electronic nature of inverter-based resources, it is important to have flexible yet clear requirements for how these resources should behave. Leaving requirements vague or incomplete can lead to abnormal or even adverse behavior for the reliability of BPS[5].

1.2 Problem Definition

An IBR has a highly complex control system that is different from a synchronous generator. Also, the IBR operation is constrained by several factors, some of which are similar to the synchronous generator while others are quite different. In addition, for IBR interconnection to the grid, a grid-connected filter is required. The three main harmonic filtering topologies for IBRs are *L*, *LC*, and *LCL* filters [8]. All these factors affect the IBR *P*-*Q* capability, which is crucial for safe operation of IBRs and development of international standards as more IBRs are connected to the grid.

Many abnormal IBR operations have been reported in the literature. In [9], the author presents field records of unstable operations from grid-connected PV plants and points out that the causes of the instabilities may involve interactions among PV inverter control systems and grid impedance characteristics.

The Author in [10] shows that generation loss of Type-4 wind and solar farms has appeared many times in coincidence with routine utility-owned capacitor switching and the article indicates that the lack of a clear industry guideline has caused confusion to all involved parties.

The authors in [11] presented and analyzed a large number of protection challenges caused by abnormal IBR operations.

In addition, many recent research articles pointed out that weak grids could have caused a lot of abnormal and unstable IBR operations [12-14].

The purpose of this thesis is to provide a comprehensive P-Q capability study for IBRs considering different IBR filtering mechanisms, control characteristics, pulse-width modulation

schemes, grid voltage impact, and parameter change impact. The specific contributions of the thesis include:

1) A study on how the IBR P-Q capability is considered in building the IBR control for the IBR grid interconnection.
2) Development of the IBR output active and reactive power models for IBR control in d-q vector framework considering different filtering mechanisms.
3) Development of algorithms for computing IBR P-Q capability considering constraints that are specific to an IBR inverter and different from those for a synchronous generator.
4) Comprehensive evaluation of IBR P-Q capability curves under different conditions.
5) Electromagnetic transient (EMT) simulation to evaluate IBR abnormal operations from dynamic IBR P-Q capability perspectives.
6) P-Q capability theoretical evaluation for an L-filter IBR.

1.3 Thesis organization

The rest of the thesis is structured as follows.

Chapter 2 the basic IBR characteristics and control configuration are presented.

Chapter 3 develops IBR active and reactive power models under IBR dq vector control.

Chapter 4 the algorithms to determine IBR P-Q capability curves are developed.

Chapter 5 a comprehensive IBR P-Q capability evaluation is given.

Chapter 6 further presents a theoretical P-Q capability study for an L-filter based IBR.

Chapter 7 the derivation of P-Q capability curve equation.

Chapter 8 the thesis concludes with summary remarks.

2. INVERTER-BASED RESOURCES, GRID INTERCONNECTION AND CONTROL

Inverter-based resources pose benefits as well as challenges for BPS, and the industry is faced with a growing penetration of these resources connected to the BPS. Inverter-based resource response to grid conditions is dominated by advanced controls programmed into the inverters and plant-level controls. These controls are configurable and capable of providing similar ERS as synchronous generating resources. However, the challenge centers on ensuring clear and consistent performance specifications for these resources since their response is driven predominantly by controls rather than the physical design of the equipment. [5].

2.1 Inverter-based resources

An IBR generally is interfaced to BPS via one or more power electronic inverters. Typical IBRs include variable speed doubly-fed induction generator (DFIG) wind turbine (Type 3), variable speed permanent magnet synchronous generator (PMSG) wind turbine (Type 4), solar photovoltaic (PV) generator, and battery energy storage (including electric vehicle charging stations) [12-15]. Except for the Type 3 wind turbine, others are normally interfaced to the BPS via a full-scale dc/ac inverter as shown in Figure 2.1, which is the focus of this thesis.

For a Type 4 wind turbine and solar PV generator, the active power always flows from an IBR unit to the BPS, but for a battery energy storage and charging station, the active power can flow either from an IBR to the BPS for discharging or from the BPS to the IBR for charging.

For all these full inverters interfaced IBRs, the reactive power is bidirectional, i.e., either generating from an IBR to the BPS or absorbing from the BPS to the IBR. For all, the active and reactive power transferred between an IBR and the BPS depends on how an IBR is controlled.

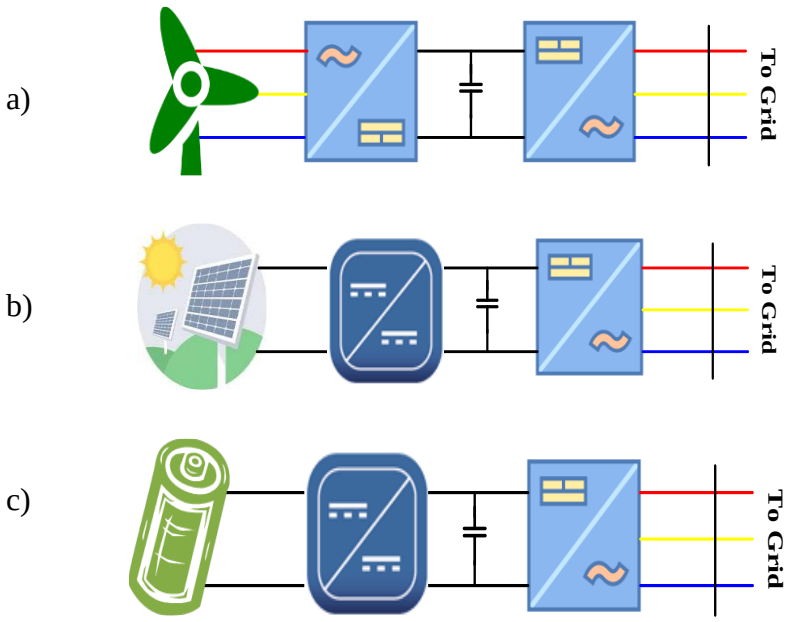

Fig. 2.1 Full inverter interfaced IBRs: a) Type 4 wind turbine, b) Solar PV generator, c) Battery energy storage

2.2 Solar energy

Photovoltaic power supplied to utility grid become more and more important part in renewable source. PV cell is an all electrical device by absorbing energy by sunlight to produce electrical power. A PV module is made up of around 36 or 72 cells connected in series. The PV cell produce a DC electrical power and need transfer to AC power to connect the grid. Fig 2.2 is a general block diagram of a grid connected PV system.

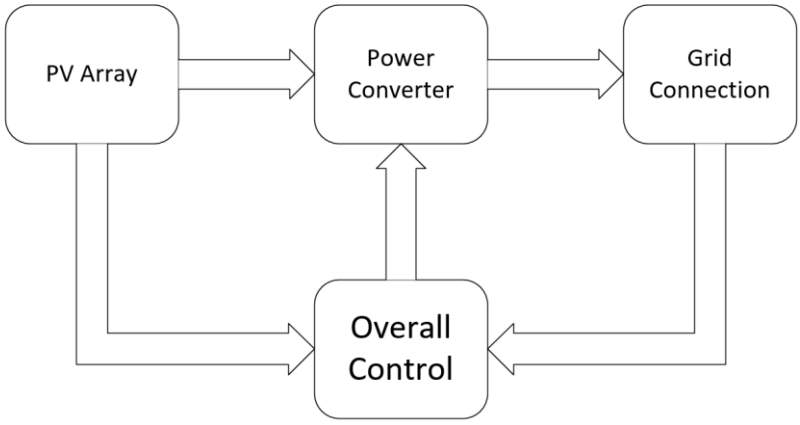

Fig 2.2 Block diagram of a single-phase grid connected PV system including control

The PV array can be a single panel, a string of PV panels or a multitude of parallel string of PV panels. There are three kinds of main topology for the PV system, they are central inverters, string inverter and module integrated inverter. Central inverters are arranged in many parallel strings that are connected to a single central inverter on the DC-side. The central inverter is lower cost for system, but the energy yield of PV plant decreases due to module mismatching and potential partial shading conditions. Similar to the central inverter, the PV plant can divide into some parallel strings, each string is connected to a string inverter. The strings inverter have capability of separate Maximum power point tracking of each PV sting. It can reduce the module mismatching and potential shading losses. Module intergrade inverter method is using an inverter for each module. This topology can optimize the adaptability of the inverter to PV characteristics. The structures for PV system show as Fig 2.3.

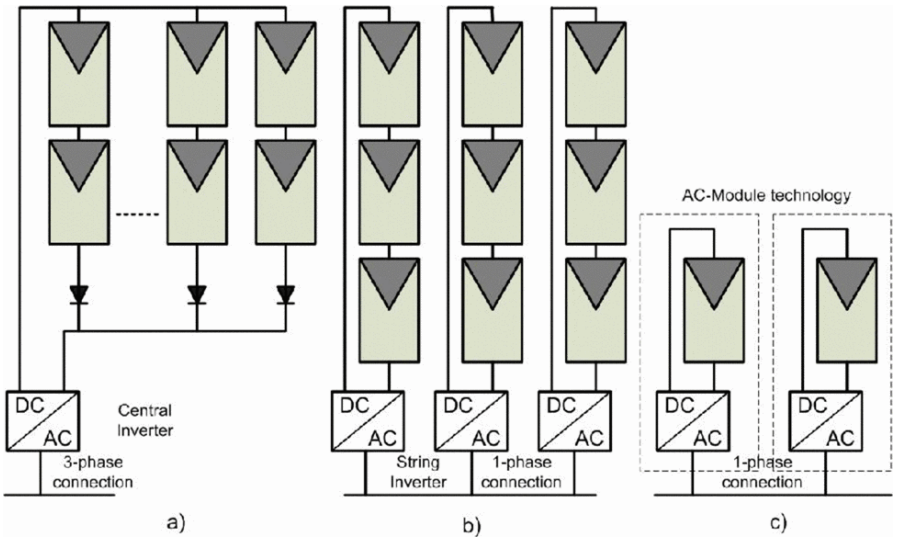

Fig 2.3 Structures for PV systems: a) Central inverter, b) String inverter and c) Module integrated inverter.[27]

For the grid connected PV inverter, the most common control structure for the dc/ac grid converter is using a current controlled H bridge PWM with a filter. The use LCL filter design is show as Fig 2.4

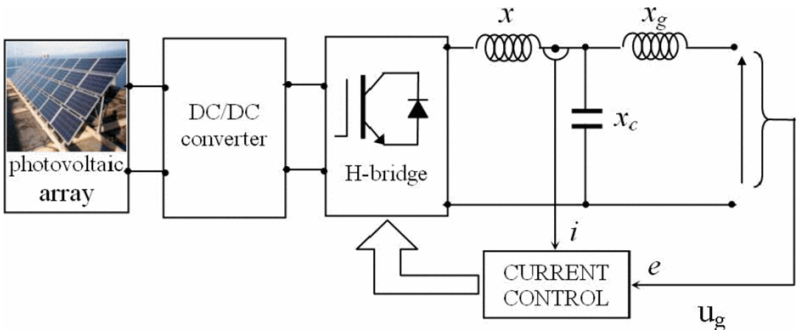

Fig 2.4 H bridge PV converter with LCL filter[27]

2.3 Wind energy

Wind turbine is one of the most important IBR, which capture power from wind by the fan blades and convert it to rotating mechanical power. There are four to five generations of wind turbines exist and it is now proven technology. It needs to control and limit the converted mechanical power at higher wind speed. The wind turbine system developed from without power

electronics to with partially rated power electrics and full-scale power electronic interfaced. Nowadays, most used wind turbine system is the full-scale power converter between the generator and grid. Fig 2.3 shows four familiar full-scale power electronic wind turbine system.

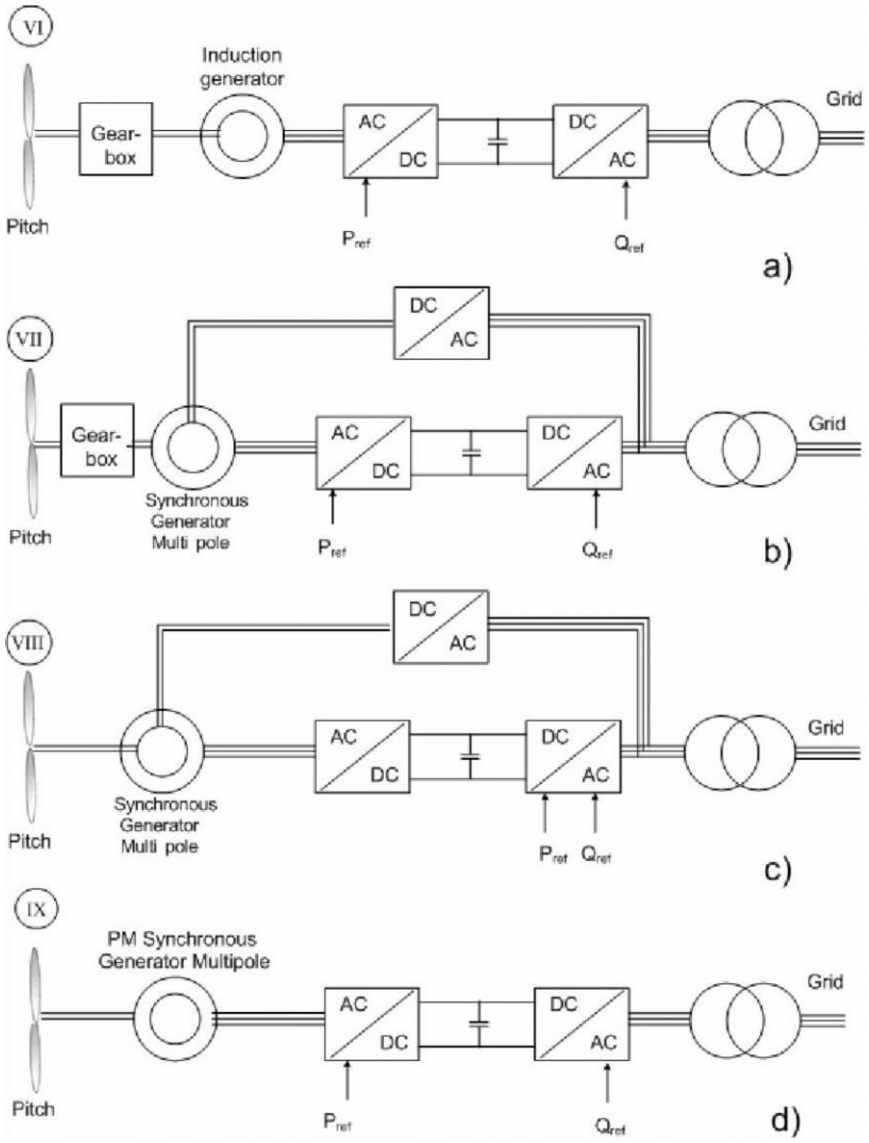

Fig. 2.5 Wind turbine systems with full-scale power converter: a) Induction generator with gearbox, b) Synchronous generator with gearbox, c) Multi-pole synchronous generator, d) Multi-pole permanent magnet synchronous generator [28]

Fig 2.5a and Fig 2.5b have a gear box, the Fig 2.5b by the synchronous generator needs a small power converter to excited field. Fig 2.5c and Fig 2.5d are multipole system with the

synchronous generator without gear box and the Fig 2.5d is using PMSG which becoming cheaper and thereby more attractive. the generator is decoupled all above system have the same controllable characteristics.

Controlling a wind turbine involves both fast and slow control dynamics. The power has to be controlled by means of the aerodynamic system and has to react based on a set-point given by a dispatched center of locally with the goal to maximize the power production based on the available wind power. Fig 2.6 show the type 4 wind system, which is industrially used today. A passive rectifier and a boost converter are used in order to boost the voltage at low speed. The grid-side converter is keeping the dc link voltage fixed. Inner current loop and power loop for wind turbine control just operation as Fig 2.7b.

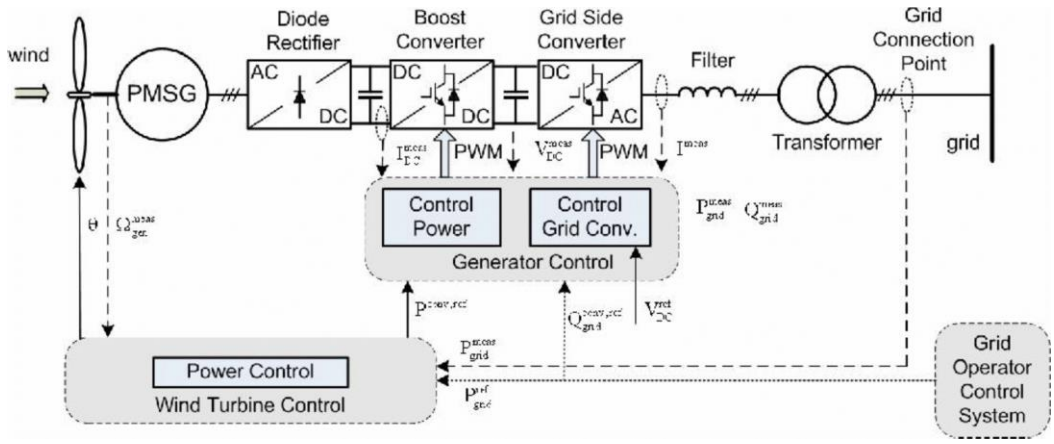

Fig 2.6 control of PMSG [28]

2.4 Energy storage

Both solar and wind energy often need battery to storage the energy, Utility-scale battery energy storage systems featuring fast response characteristics can provide an economic and promising alternative to smooth the output power of RES [29]. There are two main method

of the power electronics for the systems which are transformer based and transformerless. The transform-based topologies use 2 or 3 level converters, which is consists of 2 or 3 level converter and a line frequency transform show as Fig 2.7.

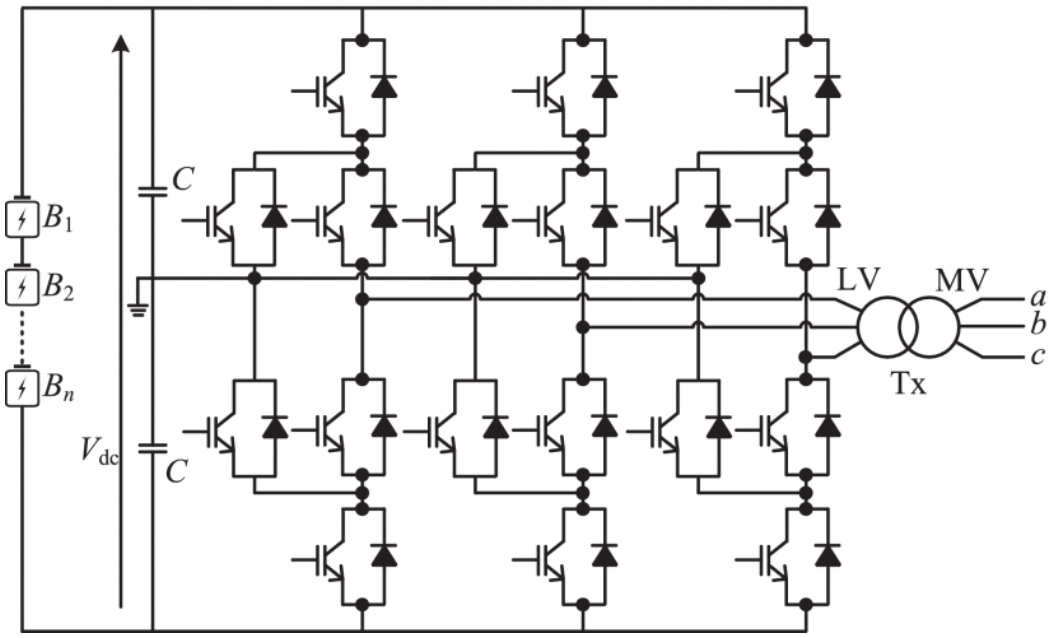

Fig 2.7 3 level converter transformer-based energy storage[29]

The line-frequency transformer used in the previously described PE units is bulky, lossy and costly. Therefore, the transformerless method had been developed. There is two topologies of the transformerless energy storage, series connection of semiconductors and series connection of sub-modules. For the first topologies the structure is similar to the transformer based without the transformer. This topology only working in a low switch frequency to less the switching losses. The sub-modules topology is use cascaded H-bridge converter or modular multilevel converter show as Fig 2.8.

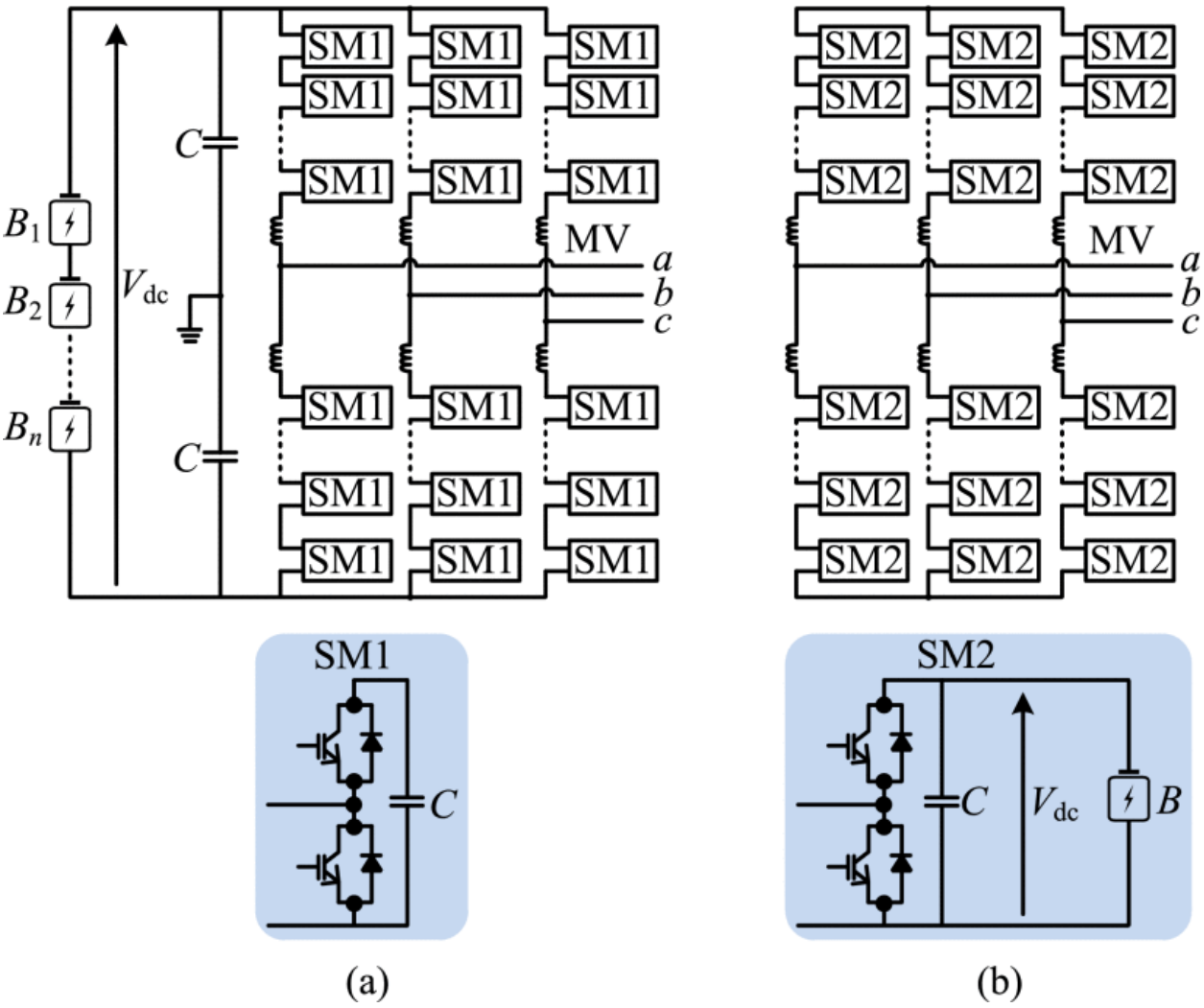

Fig 2.8 series connection of sub-modules energy storage (a) cascaded H-bridge converter (b) modular multilevel converter[29]

2.5 Control of a full inverter interfaced IBR

An IBR for wind, solar and battery storage has a common configuration as shown in Fig. 3a, which consists of an IBR-side converter, a dc-link capacitor, a grid-side converter, and a grid filter between the inverter output terminal and the point of the common coupling (PCC) with the grid [12-15]. The IBR-side converter is typically an ac/dc converter for a Type-4 wind and a dc/dc converter for solar and battery; the grid-side converter is a dc/ac inverter. The task of the controller applied to the IBR-side converter is for power extraction from wind/solar or for energy

management of battery; the task of the controller applied to the grid-side inverter is to maintain a constant dc-link voltage and regulate reactive power according to a grid demand. For an IBR as a whole to the grid, it is equivalent to assume that the dc-link voltage is constant while the controller of the grid-side inverter (Fig. 2.1b) has a cascaded inner-loop current controller plus an outer-loop active and reactive power controller, usually designed in the dq reference frame based on the PCC voltage orientation. The outer-loop power controller generates d- and q-axis reference currents and the inner-loop current controller generates d- and q-axis control voltages, v*d_inv and v*q_inv. The voltage injected to the BPS at the inverter terminal vdq_inv is related to the control voltage as follows [16],

$$v_{dq\_inv} = k_{PWM} \cdot v^{*}_{dq\_inv} \qquad (1)$$

where PWM represents the ratio of the IBR terminal voltage to the controller output voltage resulted from the pulse width modulation (PWM) [16].

The purpose of the outer-loop power controller is to adjust the IBR output active and reactive powers at the PCC to follow the reference active and reactive powers, P^{*}_{PCC} and Q^{*}_{PCC}, at the steady state. To assure the safe operation of an IBR, the reference power commands presented to the controller in Fig. 3b must be within the *P*-*Q* capability region that is permissible by the IBR inverter due to the physical constraints of the inverter.

a)

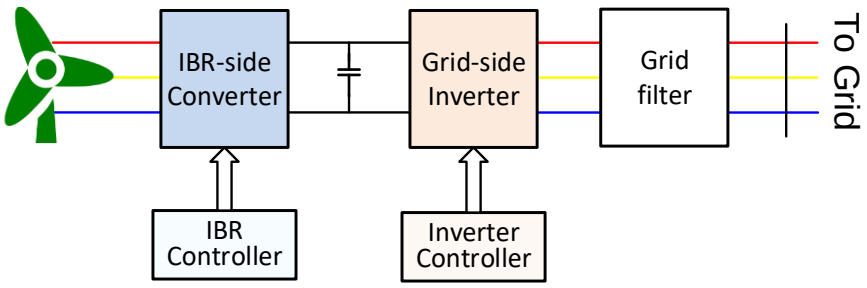

b)

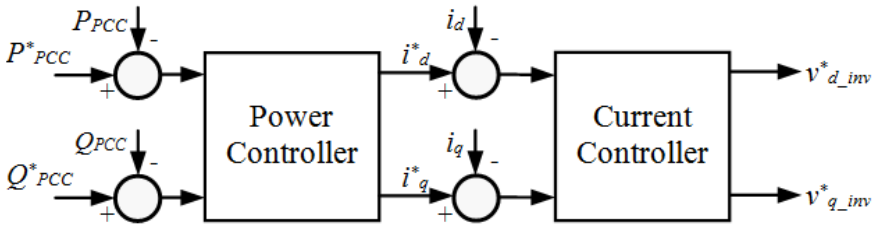

Fig. 2.9 Control of full inverter interfaced IBR: a) IBR as well as IBR controllers, b) Equivalent IBR inverter controlle

3. IBR INVERTER P-Q MODEL IN DQ REFERENCE FRAME UNDER DIFFERENT FILTERS

In order to gain the P-Q capability curves of an IBR, P-Q models of an IBR inverter needs to be obtained, which should be developed by considering IBR control characteristics as described above. As shown in Chapter 2, the controller of the IBR inverter is designed in a *dq* reference frame and the purpose of the outer-loop power controller is to regulate IBR output power at the steady-state to the reference active and reactive power. Hence, to understand how the IBR *P*-*Q* capability should be considered in building the IBR control for the IBR grid interconnection, it is important to derive the IBR steady-state output power model at the PCC using the same *dq* reference frame. Then, based on the IBR output power model developed in this section, we will investigate how to obtain dynamic IBR *P*-*Q* capability considering the impacts of the grid, IBR filter parameters, IBR physical constraints, etc. in the sections that follow.

On the other hands, the P-Q capability curves looking at the PCC are affected by the types of the grid-connected filters used for the BPS interconnection. Typical IBR filtering strategies include L, LC and LCL filters. As a result, P-Q models should be derived by considering the three different filtering mechanisms.

3.1 P-Q model of an L-filter based IBR

Table 3.1 The symbols in L-filter based IBR

R_f L_f	the resistance and inductance of the grid-connected filter
v_{a_inv} v_{b_inv} v_{c_inv}	the IBR inverter terminal voltage in the three-phase ac system
v_{d_inv} v_{q_inv}	the corresponding voltages in the dq-reference frame
$v_{a,b,c}$	the three-phase PCC voltage
v_d v_q	the corresponding voltage in the dq-reference frame
$i_{a,b,c}$	the three-phase current flowing through the L-filter to the BPS
i_d i_q	the corresponding current in the dq-reference frame

Table 3.1 and Fig. 3.1 show the schematic of an IBR with an L-filter for the grid interconnection, in which R_f and L_f are the resistance and inductance of the grid-connected filter, v_{a_inv}, v_{b_inv}, v_{c_inv} represents the IBR inverter terminal voltage in the three-phase ac system and the corresponding voltages in the dq-reference frame are v_{d_inv} and v_{q_inv}, $v_{a,b,c}$ is the three-phase PCC voltage and the corresponding voltage in the dq-reference frame are v_d and v_q, $i_{a,b,c}$ is the three-phase current flowing through the L-filter to the BPS and the corresponding current in the dq-reference frame are i_d and i_q.

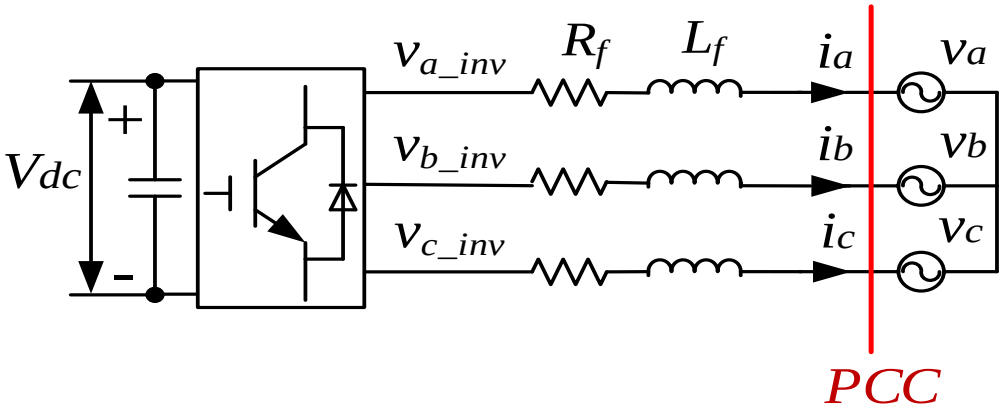

Fig. 3.1 L-filter-based grid-connected converter schematic

Using the generator sign convention, the voltage balance across the L-filter inductor in the dq reference frame is [17]

$$\begin{bmatrix} v_{a\_inv} \\ v_{b\_inv} \\ v_{c\_inv} \end{bmatrix} = R_{inv} \begin{bmatrix} i_{a\_inv} \\ i_{b\_inv} \\ i_{c\_inv} \end{bmatrix} + L_{inv} \frac{d}{dt} \begin{bmatrix} i_{a\_inv} \\ i_{b\_inv} \\ i_{c\_inv} \end{bmatrix} + \begin{bmatrix} v_a \\ v_b \\ v_c \end{bmatrix} \quad (2)$$

Transfer (2) from the abc to dq is

$$\begin{bmatrix} v_{d\_inv} \\ v_{q\_inv} \end{bmatrix} = R_f \begin{bmatrix} i_d \\ i_q \end{bmatrix} + L_f \frac{d}{dt} \begin{bmatrix} i_d \\ i_q \end{bmatrix} + \omega_s L_f \begin{bmatrix} -i_q \\ i_d \end{bmatrix} + \begin{bmatrix} v_d \\ v_q \end{bmatrix} \quad (3)$$

where ω_s is the angular frequency of the BPS voltage. In terms of dq vectors, (3) is expressed by a complex equation (4) in which v_{dq}, i_{dq}, and v_{dq_inv} are instantaneous dq vectors of the PCC voltage, grid current, and IBR inverter output voltage in the dq reference frame.

$$v_{dq\_inv} = R_f \cdot i_{dq} + L_f \frac{d}{dt} i_{dq} + j\omega_s L_f \cdot i_{dq} + v_{dq} \quad (4)$$

In the steady-state condition, (4) becomes (5), where V_{dq}, I_{dq} and V_{dq_inv} denote the steady-state dq vectors of PCC voltage, line current, and inverter output voltage.

$$V_{dq\_inv} = R_f \cdot I_{dq} + j\omega_s L_f \cdot I_{dq} + V_{dq} \quad (5)$$

Using PCC voltage orientation [15], we have $V_{dq} = V_d + j0$ if the d-axis of the reference frame is aligned along the grid PCC voltage. Assume $V_{dq\_inv} = V_{d\_inv} + jV_{q\_inv}$. Then, the current flowing between the BPS and the IBR according to (5) is

$$I_{dq} = \frac{V_{dq\_inv} - V_{dq}}{Z_f} = \frac{V_{d\_inv} - V_d}{Z_f} + \frac{jV_{q\_inv}}{Z_f} \quad (6)$$

where $Z_f = R_f + j\omega_s L_f$ stands for the grid filter impedance.

The power flowing from the IBR to the BPS can be achieved from the complex power equation,

$$P_{PCC} + jQ_{PCC} = V_{dq} I_{dq}^{*} = V_d I_{dq}^{*} \tag{7}$$

If neglecting L-filter resistor R_f, the power flowing from the IBR to the BPS is

$$\begin{aligned} P_{PCC} &= \frac{V_d V_{q\_inv}}{X_f} \\ Q_{PCC} &= \frac{V_d}{X_f}\left(V_{d\_inv} - V_d\right) \end{aligned} \tag{8}$$

According to (8), the active and reactive powers, P_{PCC} and Q_{PCC}, transferred from the IBR to the BPS are controlled through q- and d-axis components, V_{q_inv} and V_{d_inv}, of the IBR output voltage injected into the BPS, respectively.

3.2 P-Q model of an LC-filter based IBR

Table 3.2 the symbols in LC-filter based IBR

R_f L_f	the resistance and inductance of the grid-connected filter
v_{a_inv} v_{b_inv} v_{c_inv}	the IBR inverter terminal voltage in the three-phase ac system
v_{d_inv} v_{q_inv}	the corresponding voltages in the dq-reference frame
$v_{a,b,c}$	the three-phase PCC voltage
v_d v_q	the corresponding voltage in the dq-reference frame
$i_{a,b,c}$	the three-phase current flowing through the L-filter to the BPS
i_d i_q	the corresponding current in the dq-reference frame
i_{a_inv} i_{b_inv} i_{c_inv}	the three-phase IBR output current through the LC-filter inductor
i_{d_inv} i_{q_inv}	the corresponding current in the dq-reference frame
C	the LC-filter capacitor

Table. 3.2 and Fig. 2.2 shows the schematic of an IBR with an LC-filter, in which C stands for the LC-filter capacitor, $i_{a\_inv,}$ $i_{b\_inv,}$ i_{c_inv} are the three-phase IBR output current through the LC-filter inductor and the corresponding current in the dq-reference frame are i_{d_inv} and i_{q_inv}, and other terms are the same as those described in Chapter 3.1.

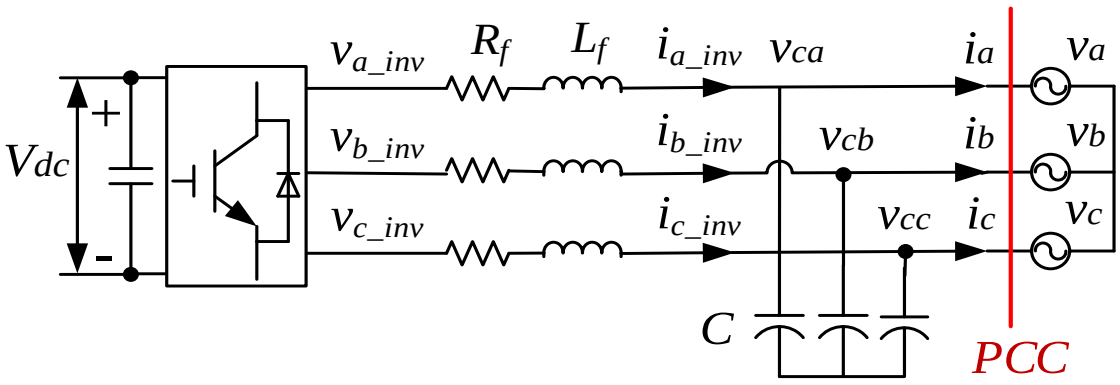

Fig. 3.2. LC-filter-based grid-connected converter schematic

Then, the voltage balance over the LC-filter inductor is (9) while the current balance over the LC-filter capacitor is (104)

$$\begin{bmatrix} v_{a\_inv} \\ v_{b\_inv} \\ v_{c\_inv} \end{bmatrix} = R_{inv} \begin{bmatrix} i_{a\_inv} \\ i_{b\_inv} \\ i_{c\_inv} \end{bmatrix} + L_{inv} \frac{d}{dt} \begin{bmatrix} i_{a\_inv} \\ i_{b\_inv} \\ i_{c\_inv} \end{bmatrix} + \begin{bmatrix} v_a \\ v_b \\ v_c \end{bmatrix} \tag{9}$$

$$\begin{bmatrix} i_{a\_inv} \\ i_{b\_inv} \\ i_{c\_inv} \end{bmatrix} = \begin{bmatrix} i_a \\ i_b \\ i_c \end{bmatrix} + C \frac{d}{dt} \begin{bmatrix} v_{ca} \\ v_{cb} \\ v_{cc} \end{bmatrix} \tag{10}$$

Transfer (9) and (10) from the abc to dq is

$$\begin{bmatrix} v_{d\_inv} \\ v_{q\_inv} \end{bmatrix} = R_f \begin{bmatrix} i_{d\_inv} \\ i_{q\_inv} \end{bmatrix} + L_f \frac{d}{dt} \begin{bmatrix} i_{d\_inv} \\ i_{q\_inv} \end{bmatrix} + \omega_s L_f \begin{bmatrix} -i_{q\_inv} \\ i_{d\_inv} \end{bmatrix} + \begin{bmatrix} v_d \\ v_q \end{bmatrix} \tag{11}$$

$$\begin{bmatrix} i_{d\_inv} \\ i_{q\_inv} \end{bmatrix} = \begin{bmatrix} i_d \\ i_q \end{bmatrix} + C \frac{d}{dt} \begin{bmatrix} v_d \\ v_q \end{bmatrix} + C\omega_s \begin{bmatrix} -v_q \\ v_d \end{bmatrix} \tag{12}$$

Using dq vectors, (11) and (12) can be expressed by (13) and (14) in which i_{dq_inv} is the dq vector of the instantaneous current through the LC-filter inductor in the dq reference reframe.

$$v_{dq\_inv} = R_f \cdot i_{dq\_inv} + L_f \frac{d}{dt} i_{dq\_inv} + j\omega_s L_f \cdot i_{dq\_inv} + v_{dq} \tag{13}$$

$$i_{dq\_inv} = i_{dq} + C\frac{d}{dt}v_{dq} + j\omega_s C \cdot v_{dq} \tag{14}$$

In the steady-state condition, (13) and (14) become (15) and (16), where I_{dq_inv} denote the steady-state space vector of the LC-filter inductor current in the dq reference reframe.

$$V_{dq\_inv} = R_f \cdot I_{dq\_inv} + j\omega_s L_f \cdot I_{dq\_inv} + V_{dq} = Z_f \cdot I_{dq\_inv} + V_{dq} \tag{15}$$

$$I_{dq\_inv} = I_{dq} + j\omega_s C \cdot V_{dq} = I_{dq} + j \cdot V_{dq} / X_C \tag{16}$$

In (15), $X_C=1/(\omega_s C)$. Thus, the steady state current flowing from the IBR to the BPS at the PCC is solved as follows

$$I_{dq} = \frac{V_{dq\_inv} - V_{dq}}{Z_f} - j\frac{V_{dq}}{X_C} \tag{17}$$

The power flowing into the BPS at the PCC can be obtained based on the complex power equation. If neglecting the resistor R_f, the power flowing into the BPS at PCC is

$$\begin{aligned} P_{PCC} &= \frac{V_d V_{q\_inv}}{X_f} \\ Q_{PCC} &= \frac{V_d\left(V_{d\_inv} - V_d\right)}{X_f} + \frac{V_d^2}{X_C} \end{aligned} \tag{18}$$

which indicates that the IBR output active and reactive powers at the PCC are like those shown by (8) except that the reactive power is a bit more positive. Thus, under the same d-axis control voltage, the IBR reactive power at the PCC is more toward generating.

3.3 P-Q model of an LCL-filter based IBR

Table 3.3 the symbols in LCL-filter based IBR

R_f L_f	the resistance and inductance of the inverter-side inductor
R_g L_g	the resistance and inductance of the grid-side inductor
v_{a_inv} v_{b_inv} v_{c_inv}	the IBR inverter terminal voltage in the three-phase ac system
v_{d_inv} v_{q_inv}	the corresponding voltages in the dq-reference frame
$v_{a,b,c}$	the three-phase PCC voltage
v_d v_q	the corresponding voltage in the dq-reference frame
$i_{a,b,c}$	the three-phase current flowing through the L-filter to the BPS
i_d i_q	the corresponding current in the dq-reference frame
i_{a_inv} i_{b_inv} i_{c_inv}	the three-phase IBR output current through the LC-filter inductor
i_{d_inv} i_{q_inv}	the corresponding current in the dq-reference frame
C	the LC-filter capacitor
$v_{ca\ cb,cc}$	the three-phase voltage of the capacitor
v_{cd} v_{cq}	the corresponding voltage in the dq-reference frame

Table. 3.3 and Fig. 3.3 shows the schematic of an IBR with an LCL-filter, in which R_f and L_f are the resistance and inductance of the inverter-side inductor, R_g and L_g are the resistance and inductance of the grid-side inductor, $v_{ca,cb,cc}$ is the three-phase voltage of the capacitor and the corresponding voltage in the dq-reference frame are v_{cd} and v_{cq}, and others are the same as those defined in Chapter 3.2.

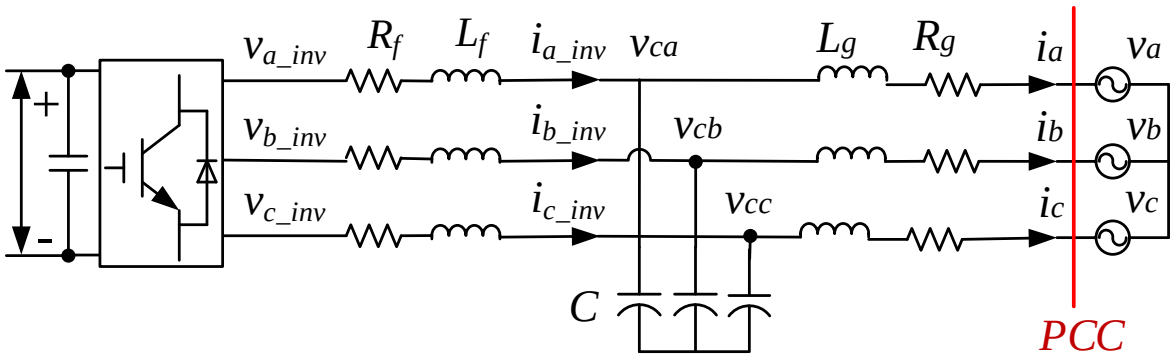

Fig. 3.3 LCL-filter-based grid-connected converter schematic

Then, the voltage equation of the grid-side inductor is

$$\begin{bmatrix} v_{ca} \\ v_{cb} \\ v_{cc} \end{bmatrix} = R_g \begin{bmatrix} i_a \\ i_b \\ i_c \end{bmatrix} + L_g \frac{d}{dt} \begin{bmatrix} i_a \\ i_b \\ i_c \end{bmatrix} + \begin{bmatrix} v_a \\ v_b \\ v_c \end{bmatrix} \tag{19}$$

Transfer (19) from the abc to dq is

$$\begin{bmatrix} v_{cd} \\ v_{cq} \end{bmatrix} = R_g \begin{bmatrix} i_d \\ i_q \end{bmatrix} + L_g \frac{d}{dt} \begin{bmatrix} i_d \\ i_q \end{bmatrix} + \omega_s L_g \begin{bmatrix} -i_q \\ i_d \end{bmatrix} + \begin{bmatrix} v_d \\ v_q \end{bmatrix} \tag{20}$$

The voltage equation of the inverter-side inductor is

$$\begin{bmatrix} v_{a\_inv} \\ v_{b\_inv} \\ v_{c\_inv} \end{bmatrix} = R_{inv} \begin{bmatrix} i_{a\_inv} \\ i_{b\_inv} \\ i_{c\_inv} \end{bmatrix} + L_{inv} \frac{d}{dt} \begin{bmatrix} i_{a\_inv} \\ i_{b\_inv} \\ i_{c\_inv} \end{bmatrix} + \begin{bmatrix} v_{ca} \\ v_{cb} \\ v_{cc} \end{bmatrix} \tag{21}$$

Transfer (21) from the abc to dq is

$$\begin{bmatrix} v_{d\_inv} \\ v_{q\_inv} \end{bmatrix} = R_f \begin{bmatrix} i_{d\_inv} \\ i_{q\_inv} \end{bmatrix} + L_f \frac{d}{dt} \begin{bmatrix} i_{d\_inv} \\ i_{q\_inv} \end{bmatrix} + \omega_s L_f \begin{bmatrix} -i_{q\_inv} \\ i_{d\_inv} \end{bmatrix} + \begin{bmatrix} v_{cd} \\ v_{cq} \end{bmatrix} \tag{22}$$

The current equation of the LCL capacitor is

$$\begin{bmatrix} i_{a\_inv} \\ i_{b\_inv} \\ i_{c\_inv} \end{bmatrix} = \begin{bmatrix} i_a \\ i_b \\ i_c \end{bmatrix} + C \frac{d}{dt} \begin{bmatrix} v_{ca} \\ v_{cb} \\ v_{cc} \end{bmatrix} \tag{23}$$

Transfer (23) from the abc to dq is

$$\begin{bmatrix} i_{d\_inv} \\ i_{q\_inv} \end{bmatrix} = \begin{bmatrix} i_d \\ i_q \end{bmatrix} + C \frac{d}{dt} \begin{bmatrix} v_{cd} \\ v_{cq} \end{bmatrix} + C\omega_s \begin{bmatrix} -v_{cq} \\ v_{cd} \end{bmatrix} \tag{24}$$

Using dq vectors, (21), (23) and (24) are expressed by (25), (26) and (27), respectively, in which v_{cdq} is the instantaneous dq vector of the LCL capacitor voltage.

$$v_{cdq} = R_g \cdot i_{dq} + L_g \frac{d}{dt} i_{dq} + j\omega_s L_g \cdot i_{dq} + v_{dq} \tag{25}$$

$$v_{dq\_inv} = R_{inv} \cdot i_{dq\_inv} + L_{inv} \frac{d}{dt} i_{dq\_inv} + j\omega_s L_{inv} \cdot i_{dq\_inv} + v_{cdq} \tag{26}$$

$$i_{dq\_inv} = i_{dq} + C \frac{d}{dt} v_{cdq} + j\omega_s C \cdot v_{cdq} \tag{27}$$

In the steady-state condition, (25), (26) and (27) become (28), (29) and (30), where V_{cdq} represents the steady-state dq vector of the LCL capacitor voltage in the dq reference reframe.

$$V_{cdq} = R_g \cdot I_{dq} + j\omega_s L_g \cdot I_{dq} + V_{dq} \tag{28}$$

$$V_{dq\_inv} = R_f \cdot I_{dq\_inv} + j\omega_s L_f \cdot I_{dq\_inv} + V_{cdq} \tag{29}$$

$$I_{dq\_inv} = I_{dq} + j\omega_s C \cdot V_{cdq} \tag{30}$$

From (28) - (30), the steady state current flowing into the BPS at the PCC is

$$I_{dq} = \frac{V_{dq\_inv} - V_{dq}\left(1 + j \cdot \frac{Z_f}{X_C}\right)}{Z_f + Z_g + j \cdot \frac{Z_f Z_g}{X_C}} \tag{31}$$

where $Z_g = R_g + j\omega_s L_g$ stands for the impedance of the grid-side inductor. If neglecting the resistors R_f and R_g, the power flowing from the IBR to the BPS at the PCC is

$$P_{PCC} = \frac{V_d V_{q\_inv}}{X_f + X_g - \frac{X_f X_g}{X_C}} \tag{32a}$$

$$Q_{PCC} = \frac{V_d\left(V_{d\_inv} - V_d\right)}{X_f + X_g - \frac{X_f X_g}{X_C}} + \frac{V_d^2 \frac{X_f}{X_C}}{X_f + X_g - \frac{X_f X_g}{X_C}} \tag{32b}$$

which indicates that the PCC active and reactive powers, like the IBRs with an L- or LC-filter, are also controlled by the IBR inverter q- and d-axis output voltages, respectively.

4. ALGORITHMS TO DETERMINE P-Q CAPABILITY CURVES

The control of an IBR inverter is limited by two factors: 1) the rated power of the inverter and 2) PWM saturation limit of the inverter. For the existing IBR inverter control methods, the reference power commends presented to the IBR controller as shown in Fig. 2.2b cannot be over these two limits. Otherwise, it would result in trips or inappropriate operation of the IBR.

4.1 Algorithm for calculating P-Q capability considering rated power/current constraint

At the nominal voltage, the IBR P-Q capability considering the rated power constraint is easy to get. Assume the rated apparent power of the IBR inverter is S_{rated}. Then, the reference power commands presented to the controller as shown in Fig. 2.2b need to satisfy the following equation:

$$\sqrt{\left(P_{PCC}^{*}\right)^{2}+\left(Q_{PCC}^{*}\right)^{2}} \le S_{rated} \tag{33}$$

where P^{*}_{PCC} can be positive (i.e. generating for wind, solar and battery storage) or negative (i.e., absorbing for battery charging), and Q^{*}_{PCC} can be positive and negative for all the three types of IBRs shown in Fig. 1.

However, if the PCC voltage is different from the nominal value, it is not appropriate to determine the P-Q capability using (33). For example, under the low-voltage ride-through condition, the actual PCC voltage will be much lower than the PCC nominal voltage, and the P-Q capability determined using (33) would result in an IBR current that is much higher than the IBR nominal or rated current. As an IBR is very sensitive to over current, instead of using (33), the P-Q capability in general situations should be determined based on the rated IBR current as follows

$$\sqrt{\left(I^*_{d\_PCC}\right)^2+\left(I^*_{q\_PCC}\right)^2} \le I_{rated} \tag{34}$$

Therefore, Algorithm 1 as shown below is developed to obtain the P-Q capability curve considering the IBR rated current constraint.

Algorithm 1: P-Q capability considering the IBR rated current constraint

1: Specify sampling number N
2: $I_{reg} = -I_{rated},\ \Delta I = 2I_{rated}/N$
3: **for** i = 1 to N
4: $I^*_d(i) = I_{reg},\ I^*_q(i) = \sqrt{\left(I_{rated}\right)^2 - \left(I^*_d\right)^2}$
5: $I^*_{dq} = I^*_d(i) + jI^*_q(i),\ \ P_{PCC+}(i) + jQ_{PCC+}(i) = V_d I^*_{dq}$
6: $I^*_{dq} = I^*_d(i) - jI^*_q(i),\ \ P_{PCC-}(i) + jQ_{PCC-}(i) = V_d I^*_{dq}$
7: $I_{reg} = I_{reg} + \Delta I$
8: **end for**
9: Draw P^*_{PCC+} over Q^*_{PCC+} curve and P^*_{PCC-} over Q^*_{PCC-} curve

4.2 Algorithm for calculating P-Q capability considering PWM saturation constraint

Firstly, the P-Q capability considering the PWM constraint depends on which PWM scheme is used by an IBR. In general, there are two PWM schemes used in an IBR inverter: sinusoidal PWM (SPWM) and space vector PWM (SVPWM) [15]. Traditionally, SPWM is used in most IBRs even though the SVPWM can result in a higher reactive power capability. For better understanding of the P-Q capability, both SPWM and SVPWM are considered in this thesis. Overall, from the PWM saturation constraint point of view, the IBR d- and q-axis control voltages injected to the BPS at the inverter terminal should satisfy the following equation:

$$\sqrt{v_{d\_inv}^2 + v_{q\_inv}^2} \le V_{dq\_\max} \tag{35}$$

where $V_{dq\_\max} = \frac{\sqrt{3}V_{dc}}{2\sqrt{2}}$ for SPWM and $V_{dq\_\max} = \frac{\sqrt{3}V_{dc}}{2}$ for SVPWM [16, 18].

Therefore, the following procedure is employed to obtain the P-Q capability curve considering IBR PWM saturation constraint: 1) start with a *dq* control voltage v_{dq_inv} whose magnitude equals to V_{dq_max}; 2) calculate I_{dq} based on (6), (17) and (31), respectively, for an IBR with L, LC, and LCL filter; 3) calculate the power transferred to the BPS at PCC through $P_{PCC} + jQ_{PCC} = V_{dq} I_{dq}^* = V_d I_{dq}^*$; 4) repeat (1) to (3) for other *dq* control voltages; 5) draw P-Q capability curve for selected *dq* control voltages. Based on the above procedure, Algorithm 2 as shown below is developed to obtain the P-Q capability curve considering the IBR PWM saturation constraint.

Algorithm 2: P-Q capability considering IBR inverter PWM saturation constraint

1: Specify sampling number N

2: $V_{reg} = -V_{dq\_\max}$, $\Delta V = 2V_{dq\_\max} / N$

3: **for** i = 1 to N

4: $V_{d\_inv} = V_{reg}$

5: $V_{q\_inv} = \sqrt{V_{dq\_\max}^2 - V_{d\_inv}^2}$, $V_{dq\_inv} = V_{d\_inv} + j \cdot V_{q\_inv}$

6: Calculate I_{dq} based on (5), (13) or (23)

7: $P_{PCC+}(i) + jQ_{PCC+}(i) = V_d I_{dq}^*$

8: $V_{q\_inv} = -\sqrt{V_{dq\_\max}^2 - V_{d\_inv}^2}$, $V_{dq\_inv} = V_{d\_inv} + j \cdot V_{q\_inv}$

9: Calculate I_{dq} based on (5), (13) or (23)

10: $P_{PCC-}(i) + jQ_{PCC-}(i) = V_d I_{dq}^*$

11: $V_{reg} = V_{reg} + \Delta V$

12: **end for**

13: Draw P_{PCC+} over Q_{PCC+} curve and P_{PCC-} over Q_{PCC-} curve

5. IBR P-Q CAPABILITY ANALYSIS

Traditionally, the *P-Q* capability of an IBR is obtained based on the nominal condition, such as nominal *PCC* voltage and nominal *dc*-link voltage. But, in real-life conditions, the grid voltage is unknown, *dc*-link voltage may change, and grid-filter parameters may be different from the nominal values. Therefore, this section focuses on studying the *P-Q* capability under both nominal and non-nominal conditions. This is named as dynamic *P-Q* capability in this paper, a new concept that is different from the traditional nominal *P-Q* capability.

An IBR inverter with the following parameters is used for the P-Q capability evaluation. 1) The rated power of the IBR inverter is 1.5MVA. 2) The *dc*-link voltage is 1500V. 3) The grid short-circuit MVA is about 37MVA; the *PCC* line voltage is 60Hz and is basically constant at 690V rms. 4) For the *L* filter, the inductance is 0.4mH and the resistance of the inductor is 0.003Ω. 5) For the *LC* filter, the inductor remains the same, and the capacitance is 25μF. 6) For the *LCL* filter, the capacitance is the same as the *LC* filter while the inductance is 0.2mH and the resistance of the inductor is 0.0015Ω for both the inverter- and grid-side inductors. Therefore, the IBR short-circuit MVA at the IBR output terminal is about 3.16MVA. All the *P-Q* capability analysis shown below is in per unit (p.u.), in which the base power and voltage are the nominal IBR power and *PCC* voltage.

Table 5.1 Parameter of IBR P-Q capability model

S_{rated}	The nominal power of the IBR inverter	1.5MVA
V_{dc}	The nominal dc-link voltage	1500V
V_{LL}	The nominal PCC line voltage	690V rms
L_f	The inductance of L/LC filter	0.4mH
R_f	The resistance of the inductor for L/LC filter	0.003Ω
C	The capacitance of LC filter	25μF
R_f R_g	The inverter-side and grid-side inductance of LCL filter	0.2mH
L_f L_g	The resistance of inverter-side and grid-side for LCL filter	0.0015Ω
f	The frequency of the PCC line voltage	60Hz

5.1 P-Q capability at the nominal condition

At the nominal condition, the PCC voltage is 1 per unit, i.e., 690V rms line-line voltage. Considering the IBR PWM saturation constraint, the maximum IBR output voltage for the nominal dc-link voltage of 1500V is $\frac{V_{dc}}{2\sqrt{2}}\Big/V_{base} = 1.3312$ per unit if SPWM is employed for the IBR inverter and is $\frac{2V_{dc}}{\pi\sqrt{2}}\Big/V_{base} = 1.5372$ per unit if SVPWM is utilized, where V_{base} represents the base phase voltage at the PCC. Therefore, the maximum inverter dq voltage V_{dq_max} in Alg. 2 would be 1.3312 and 1.5372 per unit for the SPWM and SVPWM, respectively. Before obtaining the P-Q capability curves, it is needed to convert the resistance and reactance of the grid filters into per unit too. Then, the P-Q capability curves obtained using Alg. 1 and Alg. 2 are shown in Fig. 3.2. In Fig. 3.2, one circle with the center at the point [0, 0] represents the rated IBR current circle

(RIC) while the other circles, PWML, PWMLC and PWMLCL, with the centers not at the point [0, 0] signify the IBR PWM saturation constraint boundaries for the L, LC, and LCL filters, respectively. As shown in Fig. 5.1, the IBR PWM saturation constraint circles are basically overlapped for all the three filtering schemes because the capacitor in the LC and LCL filters are mainly designed for IBR harmonic filtering purpose but not for the reactive power compensation. In general, the permissible P-Q area is the area enclosed by both the RIC and the IBR PWM saturation constraint circle. Note: under the nominal condition, RIC also represents IBR rated power circle. From Fig. 5.1, the following observations are obtained:

1) Under the nominal IBR condition specified above, the P-Q capability area is quite different from the P-Q capability of a synchronous generator and from the traditional IBR P-Q capability curves used in the industry [5-7].

2) The IBR using the SVPWM has a much larger permissible P-Q capability area than that of the IBR using the SPWM.

3) The IBR with the SPWM (Fig. 5.1a) has very limited reactive support capability (i.e., generating reactive power). Also, under the nominal condition, it is even not possible for the IBR to transfer rated active power to the grid with the SPWM. However, the IBR with the SVPWM (Fig. 8b) can greatly improve the reactive support capability even without any added cost and size of the IBR system.

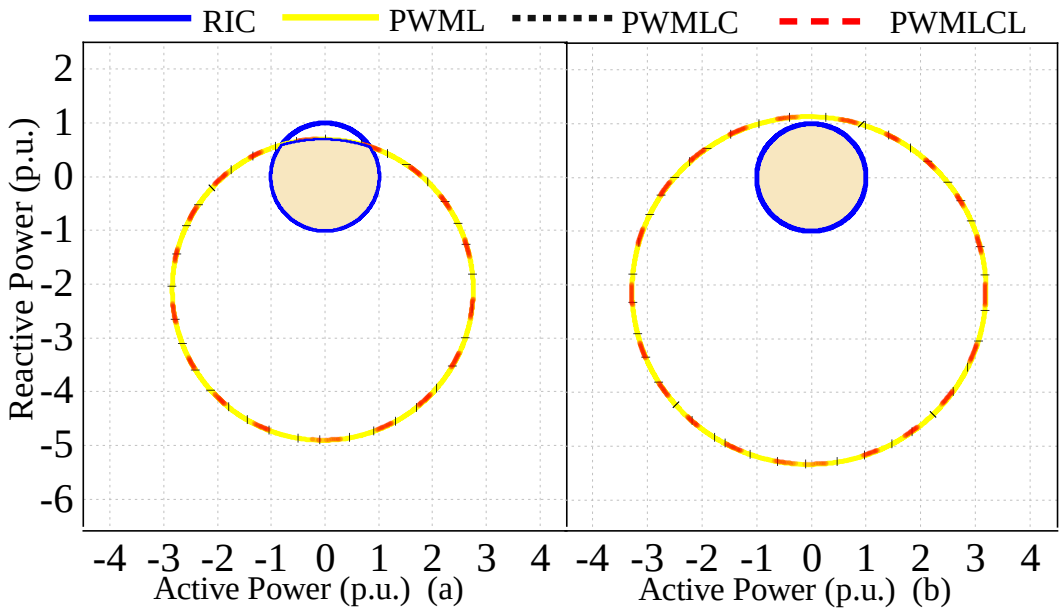

Fig. 5.1 IBR P-Q capability areas under nominal condition using (a) SPWM and (b) SVPWM

5.2 P-Q capability analysis under different dc-link and PCC voltages

According to (25) and Chapter 4, dc-link voltage and PCC voltage have important impact to the permissible IBR P-Q capability area. The dc-link voltage is usually kept constant at the nominal value via control of the grid-side inverter as shown in Fig. 1.2 while the selection of the nominal voltage is a design issue of the IBR system. On the other hand, when an IBR injects or absorbs active and reactive power into or from the grid, the PCC voltage may go up or down. To understand how the dc-link voltage and PCC voltage affect the permissible IBR P-Q capability area, an P-Q capability analysis is conducted using Alg. 1 and Alg. 2 for variable dc-link and PCC voltages as shown in Fig. 5.2. Since the difference among the IBR L, LC, and LCL filters is small, the results for the rest of Section V only focuses on the IBR with the LCL filter, the primary filtering mechanism for IBRs. From Fig. 5.2, the following characteristics are obtained:

1) The higher is the dc-link voltage, the larger is the permissible IBR P-Q capability area (Figs. 5.2a).

2) A low dc-link voltage would limit both IBR active and reactive power capability.

3) When the dc-link voltage is high enough to cause the IBR PWM saturation constraint circle enclosing the rated power circle, the permissible IBR P-Q capability area can be determined by the rated current/power circle. However, a high dc-link voltage also increases the IBR cost.

4) If the dc-link voltage remains unchanged, increasing the PCC voltage enlarges the RIC circle over the P-Q plane while the RIC circle shrinks when the PCC voltage decreases (Fig. 5.2b). This is due to the fact that under the same rated current of the inverter, the power transferred to the grid would increase for a higher PCC voltage and reduce for a lower PCC voltage. Especially, according to RIC circle in Fig. 5.2b, under the IBR low voltage ride-through condition, both the active and reactive power that can be delivered to the grid could be reduced a lot.

5) Under a constant dc-link voltage, increasing the PCC voltage would shrink the IBR PWM saturation constraint circle in the P-Q plane but increase the power delivered to the grid on the other hand according to the analysis shown in (4). Similarly, reducing the PCC voltage would enlarge the IBR PWM saturation constraint circle in the P-Q plane but reduce the power delivered to the grid. As a result, the PWM saturation constraint circles as shown in Fig. 3.3b are obtained, which would be harder to estimate in real-life conditions and thus present more challenges for IBR low- and high-voltage ride-through.

6) Again, SVPWM can give a larger permissible P-Q capability area than SPWM without any added cost.

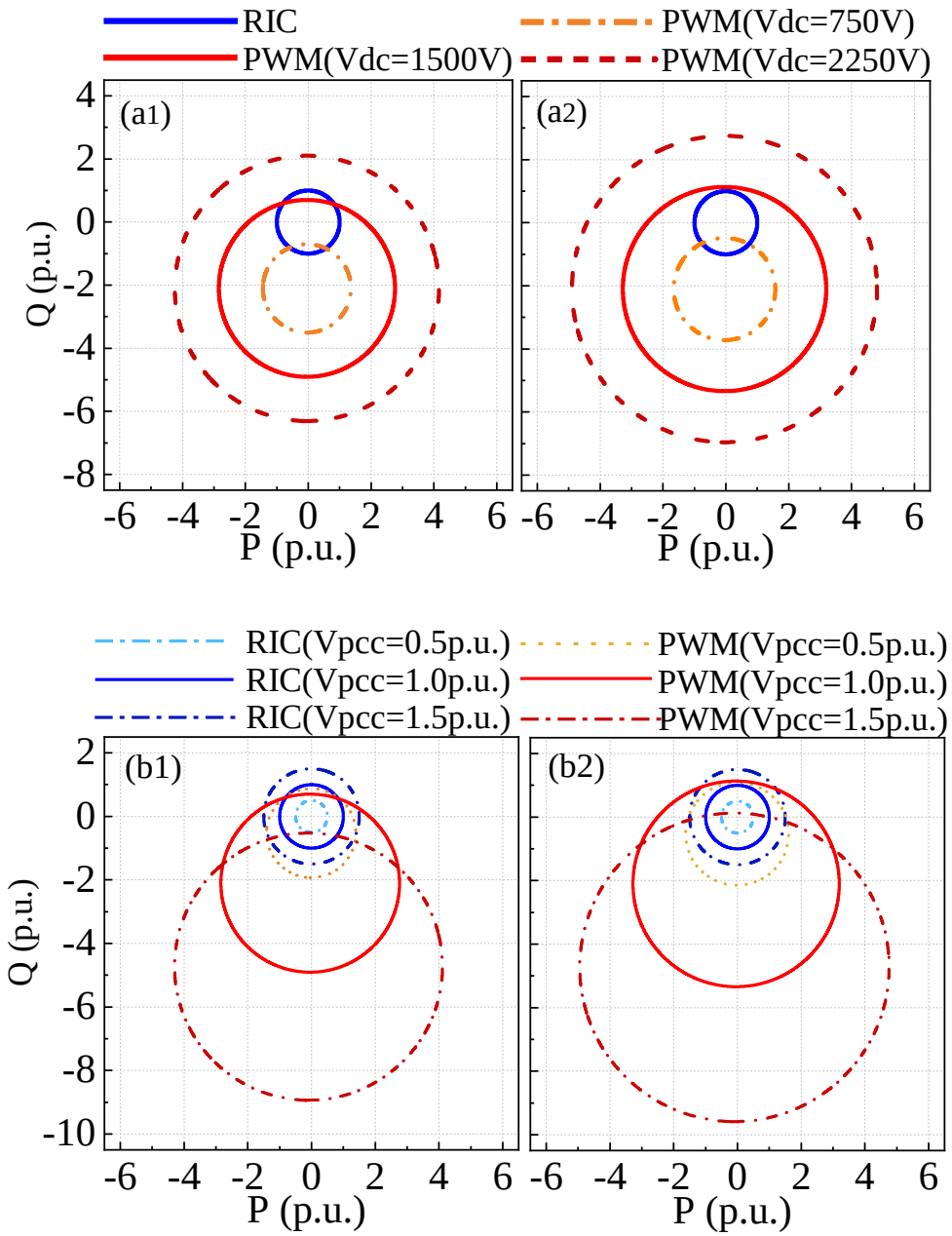

Fig. 5.2. IBR P-Q capability areas under different dc-link and PCC voltage conditions using SPWM and SVPWM

5.3 P-Q capability analysis under varying grid filter parameters

The parameters of the IBR grid-filters may change due to the temperature impact or inconsistency of the actual IBR parameters with the factory specified nominal values. It is also necessary to indicate that selection of the inductance and capacitance values is an issue to be considered at the design stage of the IBR. Both can be considered as the situation of varying grid filter parameters.

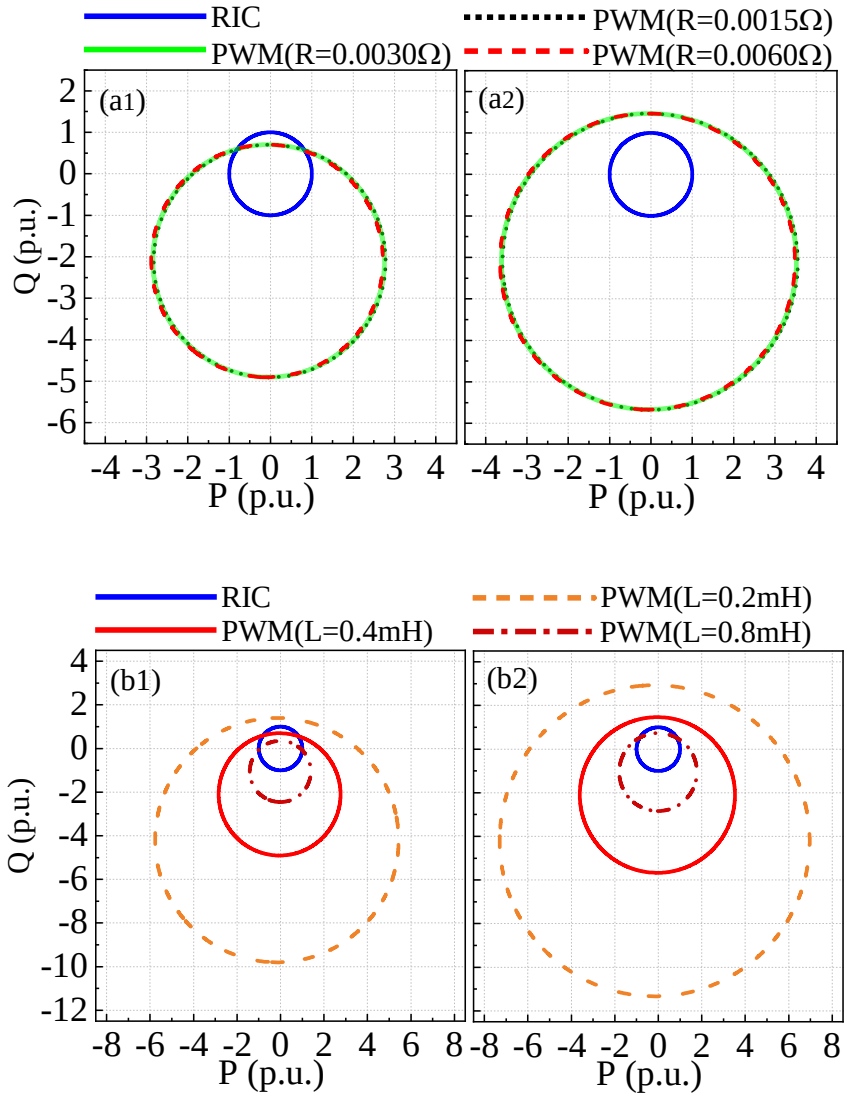

Fig. 5.3 IBR P-Q capability areas under different IBR grid filter parameters using SPWM (a1), (b1) and SVPWM (a2), (b2)

The analysis corresponding to variable IBR parameters was conducted as follows: 1) keeping the inductance at the nominal value while changing the resistance by ±50% off the nominal value, 2) keeping the resistance at the nominal value while changing the inductance by ±50% off the nominal value. Figure 8 shows the simulation results for the two specified conditions. Also, it was found that the impact of the capacitance of the grid filter is negligible and hence is not included in Fig. 5.3. From Fig. 5.3, the following characteristics are obtained:

1) As the resistance value of the grid filter changes, the RIC circle does not change but the IBR PWM saturation constraint circle shifts around a little so that the permissible IBR capability area is affected. Overall, the impact of the resistance value to the IBR P-Q capability is small.

2) As the inductance of the grid filter increases, the IBR PWM saturation constraint circle becomes smaller, which reduces both the active and reactive power capability of the IBR. According to Fig. 5.1b, the smaller the inductance value, the larger the active and reactive power capability of the IBR. However, a too small inductance value would reduce the harmonic filtering effect of the grid filter. Therefore, a proper selection of the inductance value is a design issue that needs to be considered from both the harmonic filtering and the P-Q capability perspectives.

6. MATHEMATIC DERIVATION AND ANAYSIS OF P-Q CAPABILITY CURVE EQUATION

In order to use Fig. 3.2 for any normal condition of the P-Q capability curve, this chapter will show the equation of the curve and the derivation of the equation.

Fig. 3.2 is including the rated current circle and the PWM saturation circles for L filter, LC filter and LCL filer. The RIC in per unit equation is

$$P_{rated}^2 + Q_{reted}^2 = V_d^2 I_{rated}^2 \quad (36)$$

Also, from the Fig. 3.2 the PWM saturation circles for L filter, LC filter and LCL filer almost in same position, so in this chapter the equation for the PWM saturation is base on the L filter. For the LC filter, it ignores the capacitor, and for the LCL filter, the L value will be the sum of the two indictor and the capacitor will be ignored too. For different uses and condition, this chapter will show three kinds of equation for the PWM saturation circles.

6.1 PWM saturation circle for small resister and nominal voltage

For some wind farm, the resister is very small relative to the indictor on the filer. Therefore, the resister value can be ignored as 0. Also, most time of the PCC voltage can be set as the nominal value witch often is 1 per unit value on d-component and 0 on q-component, which is $V_{dq} = 1 + 0j$. Base on the boundary value of (36) working under above condition, the equation can derivate to

$$\frac{V_{dq\max}^2}{X_f^2} = \frac{V_d^2 V_{d\_inv}^2}{X_f^2} + \left(\frac{V_d \left(V_{q\_inv} - V_d \right)}{X_f} + \frac{1}{X_f} \right)^2 \qquad (37)$$

For the above conditions the P-Q equation will be (2), and put P and Q to (26) the equation of PWM saturation circle for small resister and nominal voltage will be

$$\frac{V_{dq\max}^2}{X_f^2} = P_{PCC}^2 + \left(Q_{PCC} + \frac{1}{X_f} \right)^2 \qquad (38)$$

From (27) the circle can be defined as center at $(0, \ \frac{1}{X_f})$ and radius is $\frac{V_{dq\max}}{X_f}$.

The derivation from (36) to (38) is

$$\frac{V_{dq\max}^2}{X_f^2} = \frac{V_{q\_inv}^2}{X_f^2} + \left(\frac{V_{d\_inv}}{X_f} \right)^2$$

$$\frac{V_{dq\max}^2}{X_f^2} = \frac{V_{d\_inv}^2}{X_f^2} + \left(\frac{V_{q\_inv} - 1 + 1}{X_f} \right)^2$$

$$\frac{V_{dq\max}^2}{X_f^2} = \frac{V_{d\_inv}^2}{X_f^2} + \left(\frac{\left(V_{q\_inv} - 1 \right)}{X_f} + \frac{1}{X_f} \right)^2$$

$$\frac{V_{dq\max}^2}{X_f^2} = P_{PCC}^2 + \left(Q_{PCC} + \frac{1}{X_f} \right)^2$$

6.2 PWM saturation circle for not small resister and nominal voltage

For some filter, the resister is not small enough or the rated power and nominal voltage is not making the resister value in per unit small enough. Therefore, the resister value cannot be ignored as 0. Same as chapter 7.1, the PCC voltage still can be set as $V_{dq} = 1 + 0j$. Base on the boundary value of (36) working under above condition, the equation can derivate to

$$\frac{V_{dq\max}^2}{X_f^2+R_f^2}=\frac{\left(X_f^2+R_f^2\right)V_{d\_inv}^2}{\left(X_f^2+R_f^2\right)^2}+\frac{\left(X_f^2+R_f^2\right)V_{q\_inv}^2}{\left(X_f^2+R_f^2\right)^2} \tag{39}$$

And by expanded (31) and derivate to

$$\frac{V_{dq\max}^2}{X_f^2+R_f^2}=\left(\frac{R_f V_{d\_inv}+X_f V_{q\_inv}}{X_f^2+R_f^2}\right)^2+\left(\frac{X_f V_{d\_inv}-R_f V_{q\_inv}}{X_f^2+R_f^2}\right)^2 \tag{40}$$

Because of the resister value cannot be ignored, the P-Q equation cannot use (8), so the new P-Q equation with resister value is

$$\begin{aligned} P_{PCC}&=\frac{R_f V_{d\_inv}+X_f V_{q\_inv}-R_f}{R_f^2+X_f^2}\\ Q_{PCC}&=\frac{X_f V_{d\_inv}-R_f V_{q\_inv}-X_f}{R_f^2+X_f^2}\end{aligned} \tag{41}$$

Put P and Q to (39) the equation of PWM saturation circle for not small resister and nominal voltage will be

$$\frac{V_{dq\max}^2}{X_f^2+R_f^2}=\left(P_{PCC}+\frac{R_f}{R_f^2+X_f^2}\right)^2+\left(Q_{PCC}+\frac{X_f}{R_f^2+X_f^2}\right)^2 \tag{42}$$

From (42) the circle can be defined as center at $(-\frac{R_f}{R_f^2+X_f^2},-\frac{X_f}{R_f^2+X_f^2})$ and radius is $\frac{V_{dq\max}}{\sqrt{R_f^2+X_f^2}}$.

The derivation from (39) to (42) is

$$V_{dq\max}^2 = V_{d\_inv}^2 + V_{q\_inv}^2$$

$$\frac{V_{dq\max}^2}{X_f^2 + R_f^2} = \frac{V_{d\_inv}^2}{X_f^2 + R_f^2} + \frac{V_{q\_inv}^2}{X_f^2 + R_f^2}$$

$$\frac{V_{dq\max}^2}{X_f^2 + R_f^2} = \frac{\left(X_f^2 + R_f^2\right)V_{d\_inv}^2}{\left(X_f^2 + R_f^2\right)^2} + \frac{\left(X_f^2 + R_f^2\right)V_{q\_inv}^2}{\left(X_f^2 + R_f^2\right)^2}$$

$$\frac{V_{dq\max}^2}{X_f^2 + R_f^2} = \frac{X_f^2 V_{d\_inv}^2 + R_f^2 V_{d\_inv}^2 + X_f^2 V_{q\_inv}^2 + R_f^2 V_{q\_inv}^2}{\left(X_f^2 + R_f^2\right)^2}$$

$$\frac{V_{dq\max}^2}{X_f^2 + R_f^2} = \frac{X_f^2 V_{d\_inv}^2 + R_f^2 V_{d\_inv}^2 + X_f^2 V_{q\_inv}^2 + R_f^2 V_{q\_inv}^2 + 2R_f X_f V_{q\_inv} V_{d\_inv} - 2R_f X_f V_{q\_inv} V_{d\_inv}}{\left(X_f^2 + R_f^2\right)^2}$$

$$\frac{V_{dq\max}^2}{X_f^2 + R_f^2} = \frac{\left(R_f V_{d\_inv} + X_f V_{q\_inv}\right)^2}{\left(X_f^2 + R_f^2\right)^2} + \frac{\left(X_f V_{d\_inv} - R_f V_{q\_inv}\right)^2}{\left(X_f^2 + R_f^2\right)^2}$$

$$\frac{V_{dq\max}^2}{X_f^2 + R_f^2} = \left(\frac{R_f V_{d\_inv} + X_f V_{q\_inv}}{X_f^2 + R_f^2}\right)^2 + \left(\frac{X_f V_{d\_inv} - R_f V_{q\_inv}}{X_f^2 + R_f^2}\right)^2$$

$$\frac{V_{dq\max}^2}{X_f^2 + R_f^2} = \left(\frac{R_f V_{d\_inv} + X_f V_{q\_inv} - R_f + R_f}{X_f^2 + R_f^2}\right)^2 + \left(\frac{X_f V_{d\_inv} - R_f V_{q\_inv} - X_f + X_f}{X_f^2 + R_f^2}\right)^2$$

$$\frac{V_{dq\max}^2}{X_f^2 + R_f^2} = \left(P_{PCC} + \frac{R_f}{R_f^2 + X_f^2}\right)^2 + \left(Q_{PCC} + \frac{X_f}{R_f^2 + X_f^2}\right)^2$$

6.3 PWM saturation circle for not small resister and any voltage

In addition, same as the chapter 7.2 the resister value not set as 0. And make the equation can working in any PCC voltage value. the PCC voltage will be set as $V_{dq} = V_d + 0j$. Base on the boundary value of (36) and (39) working under above condition, the equation can derivate to

$$\frac{V_{dq\max}^2}{X_f^2 + R_f^2} = \frac{V_{d\_inv}^2}{X_f^2 + R_f^2} + \frac{V_{q\_inv}^2}{X_f^2 + R_f^2} \qquad (43)$$

Because of the voltage value become a variable, the P-Q equation cannot use (36), so the new P-Q equation with resister value is

$$P_{PCC} = \frac{R_f V_{d\_inv} V_d + X_f V_{q\_inv} V_d - R_f V_d^2}{R_f^2 + X_f^2}$$
$$Q_{PCC} = \frac{X_f V_{d\_inv} V_d - R_f V_{q\_inv} V_d - X_f V_d^2}{R_f^2 + X_f^2} \quad (44)$$

Put P and Q to (37) the equation of PWM saturation circle for not small resister and nominal voltage will be

$$\frac{V_d^2 V_{dq\max}^2}{X_f^2 + R_f^2} = \left(P_{PCC} + \frac{R_f V_d^2}{R_f^2 + X_f^2} \right)^2 + \left(Q_{PCC} + \frac{X_f V_d^2}{R_f^2 + X_f^2} \right)^2 \quad (45)$$

From (45) the circle can be defined as center at $(-\frac{V_d^2 R_f}{R_f^2 + X_f^2}, -\frac{V_d^2 X_f}{R_f^2 + X_f^2})$ and radius is $\frac{V_d V_{dq\max}}{\sqrt{R_f^2 + X_f^2}}$.

The derivation from (42) to (45) is

$$V_{dq\max}^2 = V_{d\_inv}^2 + V_{q\_inv}^2$$
$$\frac{V_{dq\max}^2}{X_f^2 + R_f^2} = \frac{V_{d\_inv}^2}{X_f^2 + R_f^2} + \frac{V_{q\_inv}^2}{X_f^2 + R_f^2}$$
$$\frac{V_{dq\max}^2}{X_f^2 + R_f^2} = \frac{\left(X_f^2 + R_f^2\right) V_{d\_inv}^2}{\left(X_f^2 + R_f^2\right)^2} + \frac{\left(X_f^2 + R_f^2\right) V_{q\_inv}^2}{\left(X_f^2 + R_f^2\right)^2}$$
$$\frac{V_{dq\max}^2}{X_f^2 + R_f^2} = \frac{X_f^2 V_{d\_inv}^2 + R_f^2 V_{d\_inv}^2 + X_f^2 V_{q\_inv}^2 + R_f^2 V_{q\_inv}^2}{\left(X_f^2 + R_f^2\right)^2}$$
$$\frac{V_{dq\max}^2}{X_f^2 + R_f^2} = \frac{X_f^2 V_{d\_inv}^2 + R_f^2 V_{d\_inv}^2 + X_f^2 V_{q\_inv}^2 + R_f^2 V_{q\_inv}^2 + 2R_f X_f V_{q\_inv} V_{d\_inv} - 2R_f X_f V_{q\_inv} V_{d\_inv}}{\left(X_f^2 + R_f^2\right)^2}$$

$$\frac{V_{dq\max}^2}{X_f^2+R_f^2}=\frac{\left(R_fV_{d\_inv}+X_fV_{q\_inv}\right)^2}{\left(X_f^2+R_f^2\right)^2}+\frac{\left(X_fV_{d\_inv}-R_fV_{q\_inv}\right)^2}{\left(X_f^2+R_f^2\right)^2}$$

$$\frac{V_{dq\max}^2}{X_f^2+R_f^2}=\left(\frac{1}{V_d}\cdot\frac{R_fV_{d\_inv}V_d+X_fV_{q\_inv}V_d}{X_f^2+R_f^2}\right)^2+\left(\frac{1}{V_d}\cdot\frac{X_fV_{d\_inv}V_d-R_fV_{q\_inv}V_d}{X_f^2+R_f^2}\right)^2$$

$$\frac{V_{dq\max}^2}{X_f^2+R_f^2}=\left[\frac{1}{V_d^2}\left(\frac{R_fV_{d\_inv}V_d+X_fV_{q\_inv}V_d-R_fV_d^2+R_fV_d^2}{X_f^2+R_f^2}\right)^2+\left(\frac{X_fV_{d\_inv}V_d-R_fV_{q\_inv}V_d-X_fV_d^2+X_fV_d^2}{X_f^2+R_f^2}\right)^2\right]$$

$$\frac{V_d^2V_{dq\max}^2}{X_f^2+R_f^2}=\left(P_{PCC}+\frac{R_fV_d^2}{R_f^2+X_f^2}\right)^2+\left(Q_{PCC}+\frac{X_fV_d^2}{R_f^2+X_f^2}\right)^2$$

6.4 Analysis

From the beginning of this chapter, (36) can draw the rated current PQ circle which is the center at the (0,0) point in the coordinate and the radius is $V_d\,I_{rated}$, when both of the PCC voltage and the rated current is 1 per unit, the curve is circle which is center at origin point and radius is 1, that same as the RIC in the Fig 5.1 and other same conditions RIC in the rest of figure in chapter 5. When the PCC voltage changed like chapter 5.2, the radius of the circle changed same as the voltage changed value. Similar as the PCC voltage, the rated current will affect the radius of the RIC same as the value change for the rated current change.

For PWM circle, the (45) show that the radius is $\frac{V_dV_{dq\max}}{\sqrt{R_f^2+X_f^2}}$, when the PCC voltage increase the radius will increase as same value. Also, the $V_{dq\max}$ is the from a linear equation with dc link voltage, so if the dc link voltage change the radius will change some ratio as the voltage change, which is same as the Fig 5.2. In addition, with the increasing of the resister and inductor value for the filter, the radius will decrease, for most of filter, the resister in per unit value is far less than the inductor, so the like the Fig 5.3, the radius affect by change of the resister is vary

small but the change of inductor almost as 1:1 radius changed. Furthermore, the center of the circle is at $(-\frac{V_d^2 R_f}{R_f^2 + X_f^2}, -\frac{V_d^2 X_f}{R_f^2 + X_f^2})$, the PCC voltage value will affect the position of the center as square level far from the origin point, but the dc link voltage will not affect the center of the circle, it is same as the Fig 5.2. Because of the value in per unit of resister and inductor is less than 1, if the value of resister or inductor increase, the center will closer to the origin point it is same as the Fig 5.3.Therefore, the equations show the same result as the algorithms in the Chapter 4 and 5.

7. IBR P-Q CAPABILITY VALIDATION VIA EMT SIMULATION

To evaluate the *P*-*Q* capability impact to the IBR safe and reliable operation, EMT simulation of a grid-connected IBR (Fig. 6.1) was realized by using SimPowerSystems. It is needed to point out that under an abnormal IBR operating condition, an IBR has to be tripped in order to prevent any damage so that the full process of the abnormal operation is usually unable to see or demonstrate via hardware experiments, which makes the EMT simulation important for such an evaluation.

In Fig. 6.1a, the grid line voltage is 34.5kV, which is connected to the IBR via an *RL* element representing the transmission line and a step-down transformer (34.5kV/690V). The IBR is connected to the transformer via an *LCL*, which can be easily modified as an *LC* or *L* filter by removing the grid-side inductor L_g and the capacitor *C*. A small passive damping resistance is added to the *LCL* capacitor to assure the stability of the *LCL*-filter-based IBR [20]. In Fig. 8a, the DER controller controls the active power extracted from the DER and sent to the grid based on a reference power command *P**, and the inverter controller controls the interconnection of the IBR with the grid.

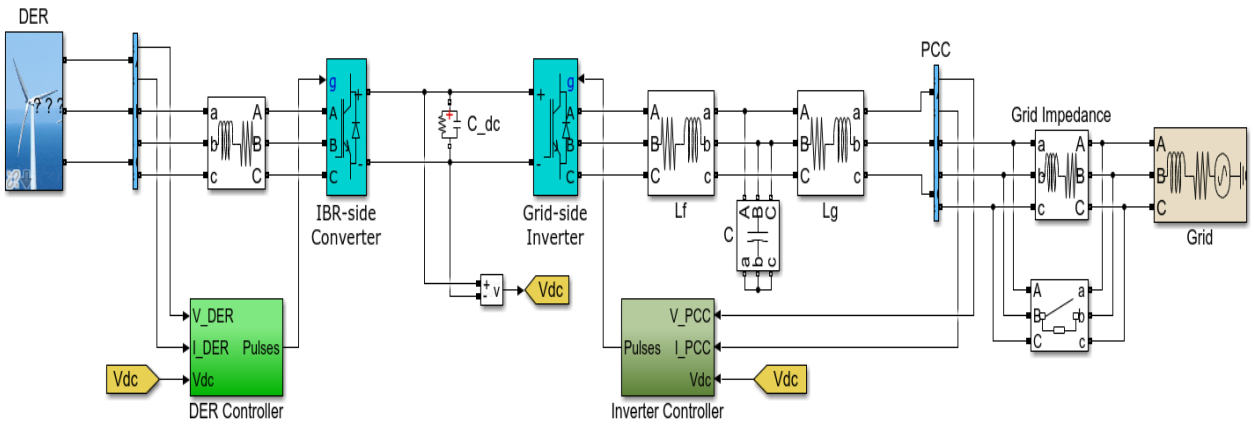

(a) EMT simulation model of the grid-connected IBR in SimPowerSystems

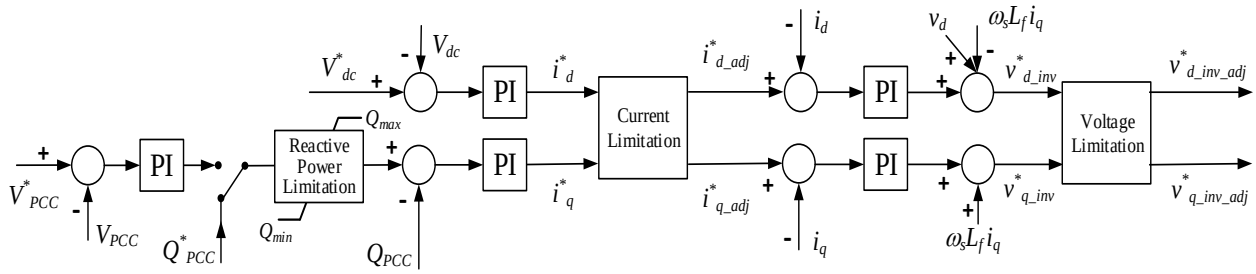

(b) Configuration of the grid-side inverter controller

Fig. 7.1 Illustration of EMT simulation model of a grid-connected IBR

7.1 Grid-side inverter controller design

Detailed configuration of the inverter controller is shown in Fig. 6.1b, which consists of an inner current controller and an outer *dc*-link voltage and *PCC* voltage or reactive power controller. The control of the *dc*-link voltage is achieved through the *d*-axis loop, and the control of the *PCC* voltage or reactive power is achieved through the *q*-axis loop. The design of the controllers follows the well-known standard vector control strategies [17, 18]. Then, the IBR capability is used to determine the safe reference commands that can be presented to an IBR considering physical constraints of the IBR. The IBR industry typically builds these into the outer- and inner-loop controllers as follows.

Frist, for the outer-loop *PCC* voltage or reactive power controller, the reactive power reference presented to the controller is limited within the nominal *P*-*Q* capability area through the reactive power limitation block applied in the q-axis loop as shown in Fig. 8b, in which Q_{max} and Q_{min} are calculated based on the reference active power command P^* and the region specified by a *P*-*Q* capability chart such as NERC (Fig. 1.2a), ERCOT (Fig. 1.2b), SPWM (Fig. 5.1a), and SVPWM (Fig. 5.1b).

Second, for the inner-loop current controller, a current limitation block is applied if $\sqrt{\left(i_d^*\right)^2+\left(i_q^*\right)^2} \geq I_{rated}$ to prevent the IBR current over the rated current limit based on the Active Power Priority Mode control according to [3, 4]

$$\begin{aligned} i_{d\_adj}^* &= i_d^* \\ i_{q\_adj}^* &= sign\left(i_q^*\right)\sqrt{\left(I_{rated}\right)^2-\left(i_d^*\right)^2} \end{aligned} \tag{46}$$

Third, to prevent IBR operating beyond the linear modulation limit, a voltage limitation block is applied to the control voltage generated by the inner-loop current controller according to [19]

$$\begin{aligned} v^*_{d\_inv\_adj} &= V_{dq\_\max} \cdot \cos\left(\angle v^*_{dq\_inv}\right) \\ v^*_{q\_inv\_adj} &= V_{dq\_\max} \cdot \sin\left(\angle v^*_{dq\_inv}\right) \end{aligned} \tag{47}$$

Finally, a saturation mechanism is applied to all the PI controllers to prevent the integral term of a PI controller from going beyond the maximum possible reactive power limit, IBR rated current limit, and IBR output voltage limit, respectively. Thus, the configuration of Fig. 8b represents the state-of-the-art IBR control technology used in the industry.

7.1.1 Current loop controller

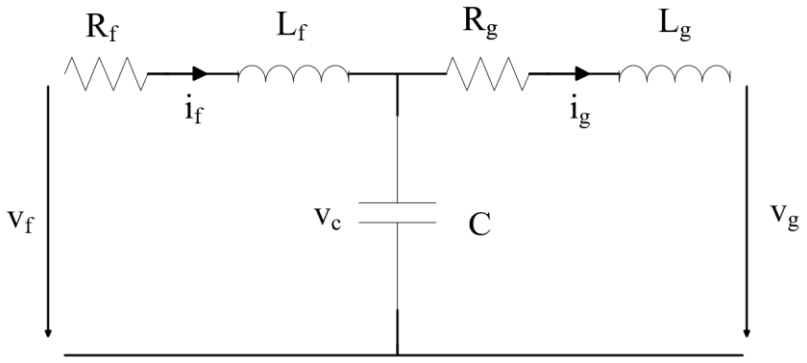

Fig 7.2 LCL filter

The current loop controller is used to produce the v_d^* and v_q^* to keep the dq voltage which use to control the PWM generator to produce the switch single for the inverter. The capacitor in the wind turbine system is very small per unit value. Therefore, for the ideal model the capacitor branch can be simple as open. There will show the detail of the LCL filter.

$$\begin{bmatrix} v_{f\_d} \\ v_{f\_q} \end{bmatrix} = R_f \begin{bmatrix} i_{f\_d} \\ i_{f\_q} \end{bmatrix} + L_f \frac{d}{dt} \begin{bmatrix} i_{f\_d} \\ i_{f\_q} \end{bmatrix} + \omega_s L_f \begin{bmatrix} -i_{f\_q} \\ i_{f\_d} \end{bmatrix} + \begin{bmatrix} v_{c\_d} \\ v_{c\_q} \end{bmatrix}$$
$$\begin{bmatrix} v_{g\_d} \\ v_{g\_q} \end{bmatrix} = -R_g \begin{bmatrix} i_{c\_d} \\ i_{c\_q} \end{bmatrix} - L_g \frac{d}{dt} \begin{bmatrix} i_{g\_d} \\ i_{g\_q} \end{bmatrix} - \omega_s L_g \begin{bmatrix} -i_{g\_q} \\ i_{g\_d} \end{bmatrix} + \begin{bmatrix} v_{c\_d} \\ v_{c\_q} \end{bmatrix} \quad (48)$$

Where i_f, and i_g are the current flow through indicator f, capacitor C and indicator g. v_c is the positive side voltage of the capacitor. v_f and v_g are the voltage of two side of the LCL filter. Because of the capacitor branch is simple as open and $i_f - i_c - i_g = 0$, i_f will equal to the i_g, (48) will same as (20) and (22). Combine with (48), the equation can be written as

$$i_{fdq} = \frac{1}{L_f s + R_f}(v_{fdq} - v_{cdq})$$
$$i_{gdq} = \frac{1}{L_g s + R_g}(v_{cdq} - v_{gdq}) \quad (49)$$

From (49) can get the the transfer function of the LCL filter,

$$G_f(s) = \frac{1}{L \cdot s + R} \quad (50)$$

Where $L=L_f + L_g$ and $R=R_f + R_g$.

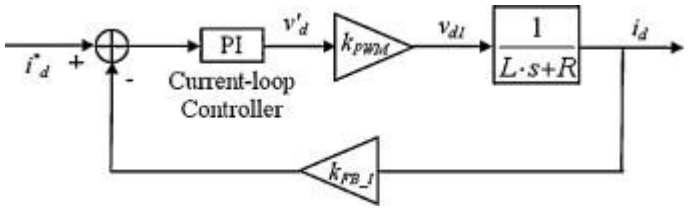

Fig 7.3 Block diagram of current loop controller

7.1.2 DC voltage controller

The DC voltage controller is used to produce the reference i_d which in order to keep the DC voltage constant. The DC voltage loop is an outer loop of the inner current loop. The internal loop have been designed to chive a short settling time to a fast correction of error. Therefor, the loop will be design slower.

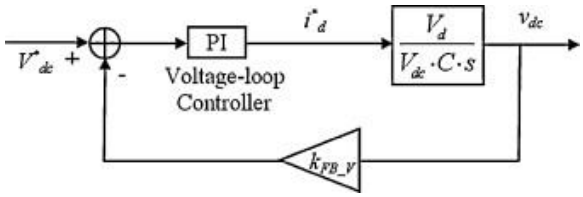

Fig 7.4 Block diagram of the DC voltage

The DC link voltage controller is based on the principle of the power balance between the ac and dc sides of inverter.[17]

$$v_{dc} i_{dc1} = v_d i_d + v_q i_q \qquad (51)$$

Where v_{dc} is the dc link voltage and i_{dc1} is the current from grid side inverter flow to the positive side of the dc link capacitor, as the d axis of the reference frame is lined along the PCC voltage position.

$$v_{dc}\left(C\frac{dv_{dc}}{dt} + i_{dc2}\right) = v_d i_d \qquad (52)$$

Where i_{dc2} is the current from the positive side of the dc link capacitor flow to the IBR side converter. If i_{dc2} is considered as a disturbance, the system block diagram as Fig. 6.3 and the transfer function is

$$G_{DC} = \frac{V_{dc}}{V_d C_{dc} s} \tag{53}$$

Where C_{dc} is the value of DC link capacitor.

7.2 Reactive power limitation model

For the EMT simulation, the boundary of outer loop reactive power model in SimPowerSystems show as the Fig 6.5. This model use to limit the maximum and minimum value of reactive power depends on required active power. The maximum and minimum boundary is processed by the block of Boundary_IBR, Boundary_NERC and Boundary_ERCOT which is calculated by the Alg. 1 by the thesis, the study by NERC and IRCOT.

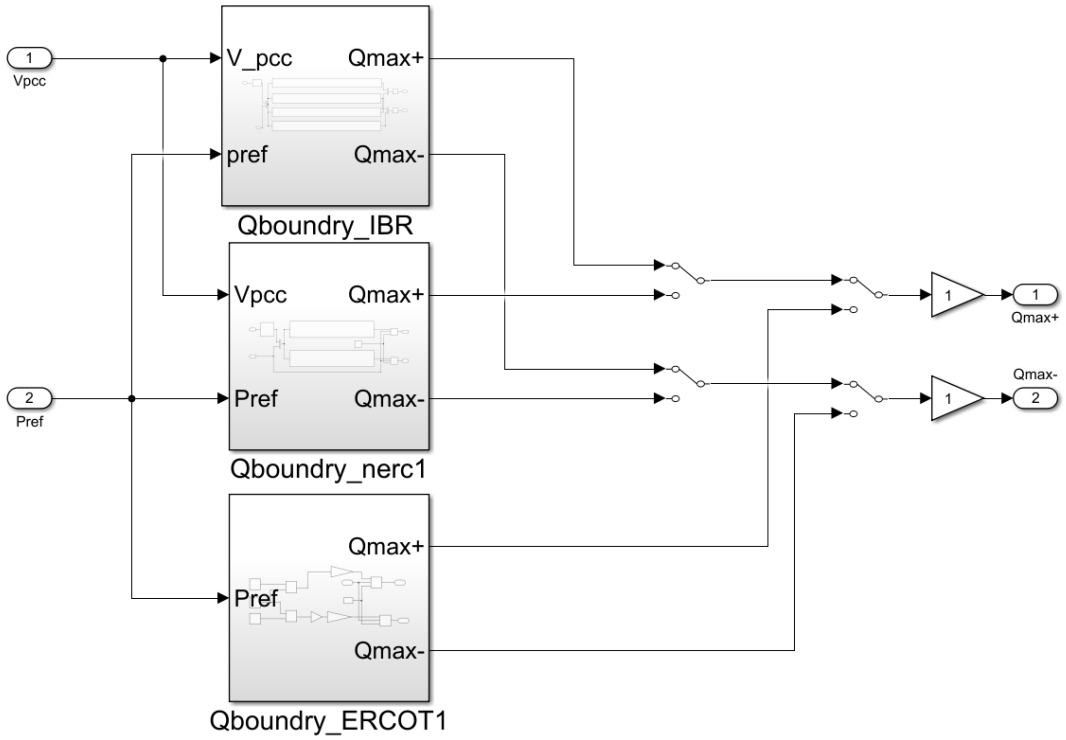

Fig 7.5 The reactive boundary model

7.2.1 The IBR boundary

The limited reactive power boundary from this thesis is calculated by the algorithm from chapter 4. There are two limited condition: the IBR rated current boundaries and the IBR PWM saturation constraint boundaries. The IBR rated current boundaries is

$$\begin{aligned} Q_{\max} &= \sqrt{\left(\sqrt{3}v_{PCC}\cdot i_{rated}\right)^2 - P_{ref}^2} \\ Q_{\min} &= -\sqrt{\left(\sqrt{3}v_{PCC}\cdot i_{rated}\right)^2 - P_{ref}^2} \end{aligned} \tag{54}$$

The v_{pcc} is the PCC voltage of the model, the i_{rated} is the rated current same as Chapter 4.1 and the P_{ref} is the required active power. The maximum and minimum boundary can draw a circle which is the RIC in Fig 5.1.

The IBR PWM saturation constraint boundaries is

$$\begin{aligned} Q_{\max} &= \frac{X_f V_{pcc}^2}{R_f^2 + X_f^2} + \sqrt{\frac{V_{pcc}^2 V_{dq\max}^2}{X_f^2 + R_f^2} + \left(P_{PCC} + \frac{R_f V_{pcc}^2}{R_f^2 + X_f^2}\right)^2} \\ Q_{\min} &= \frac{X_f V_{pcc}^2}{R_f^2 + X_f^2} - \sqrt{\frac{V_{pcc}^2 V_{dq\max}^2}{X_f^2 + R_f^2} + \left(P_{PCC} + \frac{R_f V_{pcc}^2}{R_f^2 + X_f^2}\right)^2} \end{aligned} \tag{55}$$

Where R_f and L_f are the resistance and inductance of the grid-connected filter, the maximum inverter dq voltage V_{dq_max} is determined by Alg. 2. The maximum and minimum boundary in (55) can make a circle as the PWM in Fig.5.1. Then, compare the maximum and minimum value from (53) and (54), use the smaller value of the maximum as the model maximum value and use the larger value of minimum as the model minimum value.

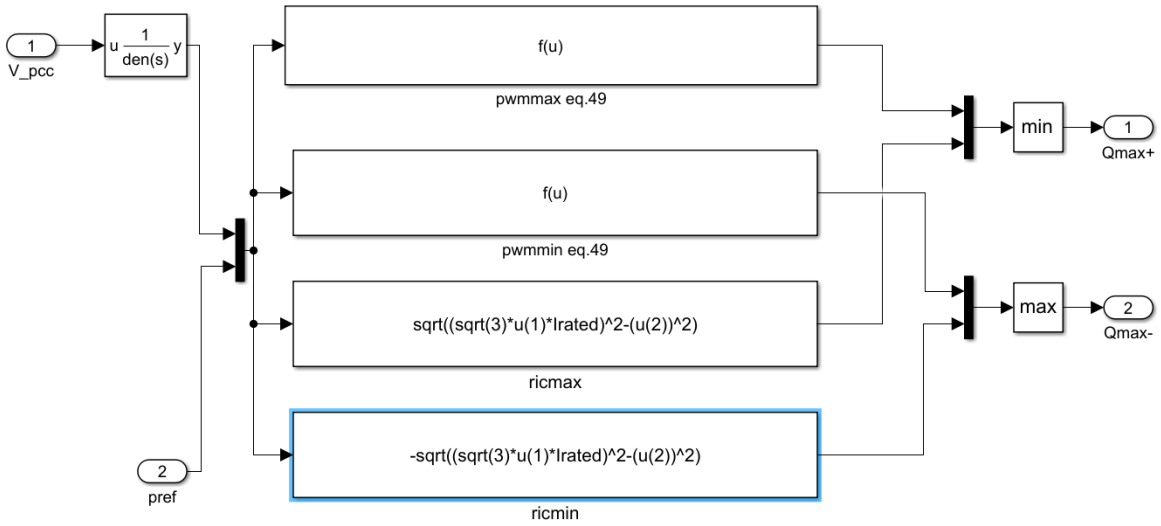

Fig 7.6 IBR boundary model

7.2.2 The NERC boundary

As the NERC Reliability Guideline in [5], from the Fig 1.2a the capability curve with near semi-circle capability and another semi-circle IBR capability curve with fixed reactive capability at around 0.95 per unit active power output levels. Therefore, the boundary equation is approximate

$$\begin{aligned} Q_{\max} &= \sqrt{\left(0.95 \cdot \sqrt{3} v_{PCC} \cdot i_{rated}\right)^2 - P_{ref}^2} \\ Q_{\min} &= -\sqrt{\left(0.95 \cdot \sqrt{3} v_{PCC} \cdot i_{rated}\right)^2 - P_{ref}^2} \end{aligned} \tag{56}$$

This is a little smaller than (43) but it can only work on positive active power.

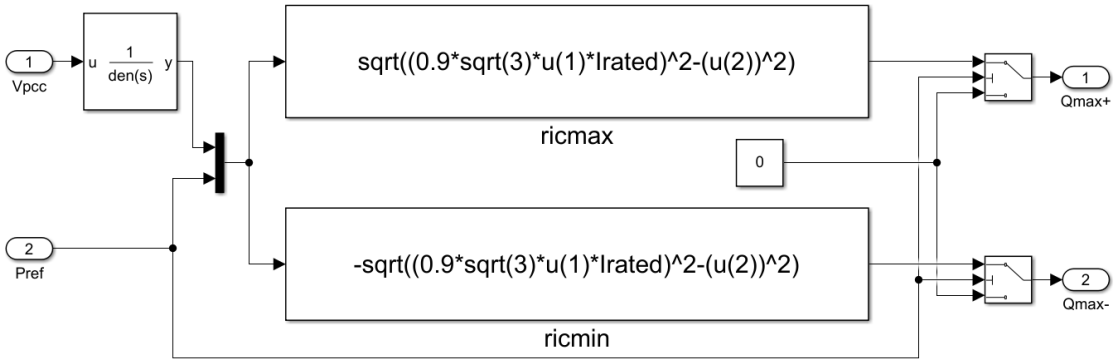

Fig 7.7 NERC boundary model

7.2.3 The ERCOT boundary

The ERCOT boundary is a rectangle P-Q capability curve that needs to meet at the Point of Interconnection. Therefore, the boundary equation is approximate

$$Q_{\max} = 0.33S_{rated}$$
$$Q_{\min} = -0.33S_{rated} \quad (57)$$

Where S_{rated} is the rated power.

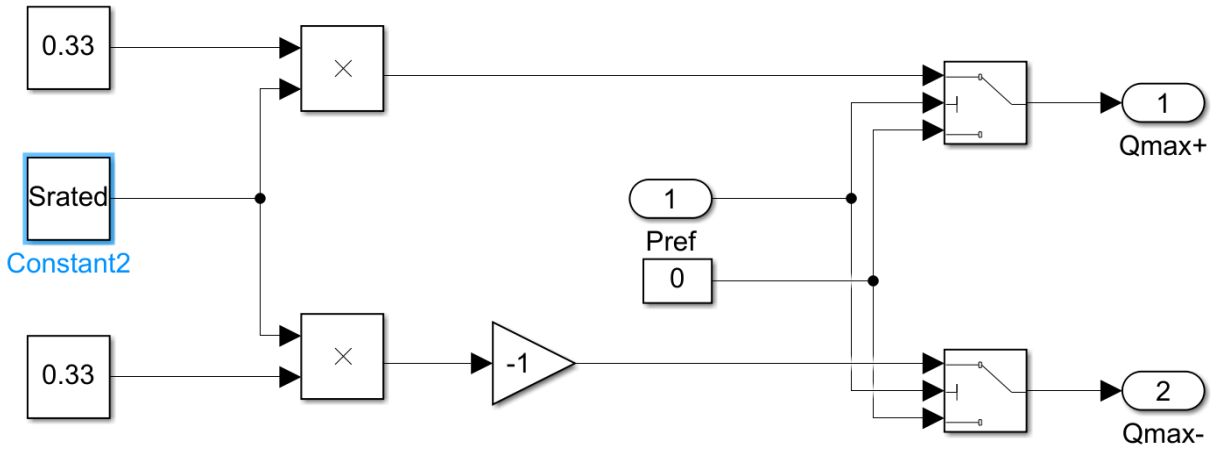

Fig 7.8 ERCOT boundary model

7.3 P-Q capability evaluation at the nominal condition

At the nominal condition, *dc*-link voltage and the IBR grid-filter parameters are set at the nominal values. The grid short-circuit MVA at the PCC is 37MVA and the *PCC* voltage is basically at the nominal value and not affected by the IBR. The active and reactive power commands presented to the IBR are limited within the *P*-*Q* capability region based on one of the following four cases: 1) SPWM with the *P*-*Q* capability of Fig. 5.1a, 2) SPWM with NERC *P*-*Q* capability (Fig. 1.2a), 3) SPWM with ERCOT *P*-*Q* capability (Fig. 1.2b), and 4) SVPWM with the P-Q capability of Fig. 5.1b.

Fig. 9 presents the simulation results, in which the *PCC* active power reference changes from 0kW to 850kW at 0.5 sec and then to 450kW at 2.5 sec. The reactive power reference changes from 400kVar to 960kVar at 1 sec. When active and reactive power references are 850kW and 400kVar before 1sec, the reference values are within the *P*-*Q* capability region for all the four cases and the IBR controller can properly regulate the *PCC* active and reactive powers to the reference values and maintain the *dc*-link voltage at 1500V.

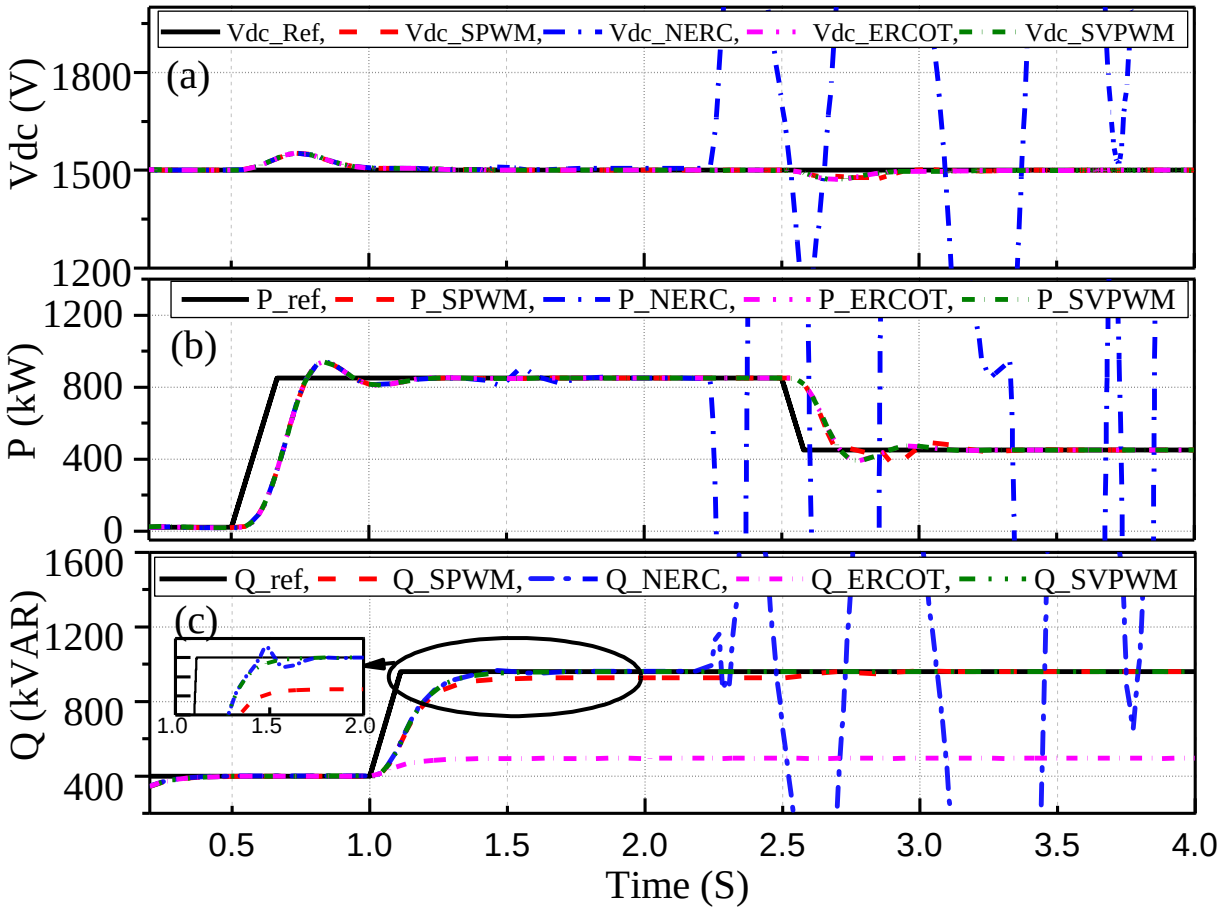

Fig. 7.9 EMT simulation for IBR P-Q capability and stability evaluation: a) dc-link voltage, b) PCC active power, c) PCC reactive power

When the active and reactive power references are 850kW and 960kVar after 1sec, the reference values are outside the *P-Q* capability regions of Cases 1 and 3 but within the *P-Q* capability regions of Cases 2 and 4. Hence, the actual reactive power reference is adjusted from 960kVar to 925kVar and 494kVar, respectively, according to the *P-Q* capability regions of Fig. 5a for Case 1 and Fig. 1b for Case 3 but remains unchanged for Cases 2 and 4. Thus, the reactive power after 1 sec is stabilized at 925kVar and 494kVar instead of 960kVar for Cases 1 and 3, respectively. As the active power reference drops to 450kW at 2.5sec, the reference values are within the *P-Q* capability region of Fig. 5.1a so that both the active and reactive power

references are followed for Case 1 but the reactive for Case 3 power still is far below the reference value showing a significant waste of the IBR capability for Case 3. For Case 2, although the reactive power after 1sec can get to the reference value initially, it eventually becomes unstable as the *P-Q* capability of Case 2 is out of the actual *P-Q* capability region shown by Fig. 5.1a, which would trip the IBR. For Case 4, the controller can maintain stable and accurate operation of the IBR for the given reference values within the simulation period, validating that an IBR with SVPWM has a larger permissible *P-Q* capability region as shown in Fig. 5.1.

7.4 P-Q capability evaluation as grid voltage changes

In real-life conditions, the voltage at the PCC can go up and down caused by a load change or fault in the grid. The IEEE 1547 requires that an IBR should have an adequate high and low voltage ride through capability. The impact of the PCC voltage is evaluated for an increase and decrease of the PCC voltage. Both can cause an abnormal operation of the IBR. Fig. 6.1 shows a case study for an increase of the *PCC* voltage from 1 p.u. to 1.2 p.u. between 1.5 sec and 2.5 sec, in which the grid short-circuit MVA is the same as that used in Fig. 7.10 and the SPWM and SVPWM nominal *P-Q* capability of Fig. 5.1a and Fig. 5.1b are used. The reference active power is 0kW and changes to 850kW at 0.5sec and the reference reactive power is 0kVar and changes to 800kVar at 1sec. It can be seen that the IBR with the SPWM becomes unable when the PCC voltage increases, which could result in a momentary cessation of the IBR. This result is consistent with Fig. 5.2 and shows the importance to consider the dynamic nature of the *P-Q* capability in the IBR control design.

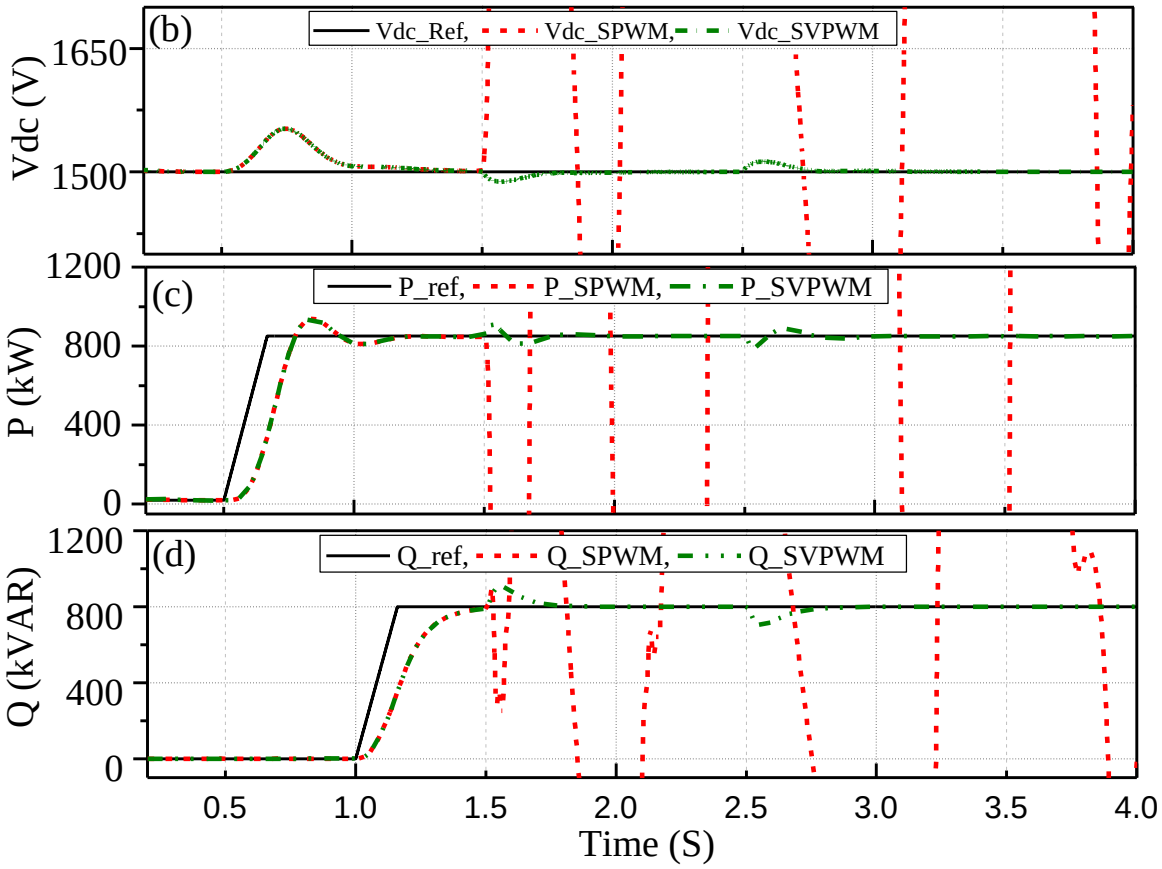

Fig. 7.10 PCC voltage impact on IBR P-Q capability and operation: a) PCC bus voltage (RMS), b) dc-link voltage, c) active power to the grid at the PCC, d) reactive power to the grid at the PCC

7.5 P-Q capability and weak grid impact

The weak grid impact may appear when an IBR is located at the end of a distribution feeder. On the other side, IEEE 1547 requires that an IBR should maintain the stability of its *PCC* voltage. Fig. 11 shows a case study of the IBR voltage control under a low-voltage ride-through condition caused by a fault. The active power reference is 400kW at 0.5sec, changes to 850kW at 2sec, and then drops to 650kW at 3sec and a fault appears at 1sec and clears at 3.5sec. The grid resistance and inductance (including the transformer) are 0.014Ω and 0.167mH, meaning that the grid short-circuit MVA at the PCC is about 7.4MVA. In the voltage control

mode, the IBR physical *P*-*Q* capability shows a more dynamic nature and is hard to determine. For the IBR control using the four *P*-*Q* capability regions as shown in Fig. 1.2 and Fig. 5.1, all except Case 3 start to increase the reactive power production after the fault and are able to maintain the PCC voltage stability at 1 p.u. For Case 2 (NERC), abnormal IBR operation presents shortly after the fault starts; for Case 1 (SPWM), abnormal IBR operation appears when the active power reference increases to 850kW at 2sec; for Case 4 (SVPWM), abnormal IBR operation starts to evolve after the active power reference drops from 850kW to 650kW at 3sec. This would cause IBR trip or momentary cessation in order for the IBR to get out of the abnormal operating conditions. For Case 3 (ECORT), the upper limit of reactive power is reached before the IBR goes into the abnormal operation which limits the maximum potential to boost the PCC voltage to 1 p.u., however, the stable and normal IBR operation is maintained during the low-voltage ride-through event.

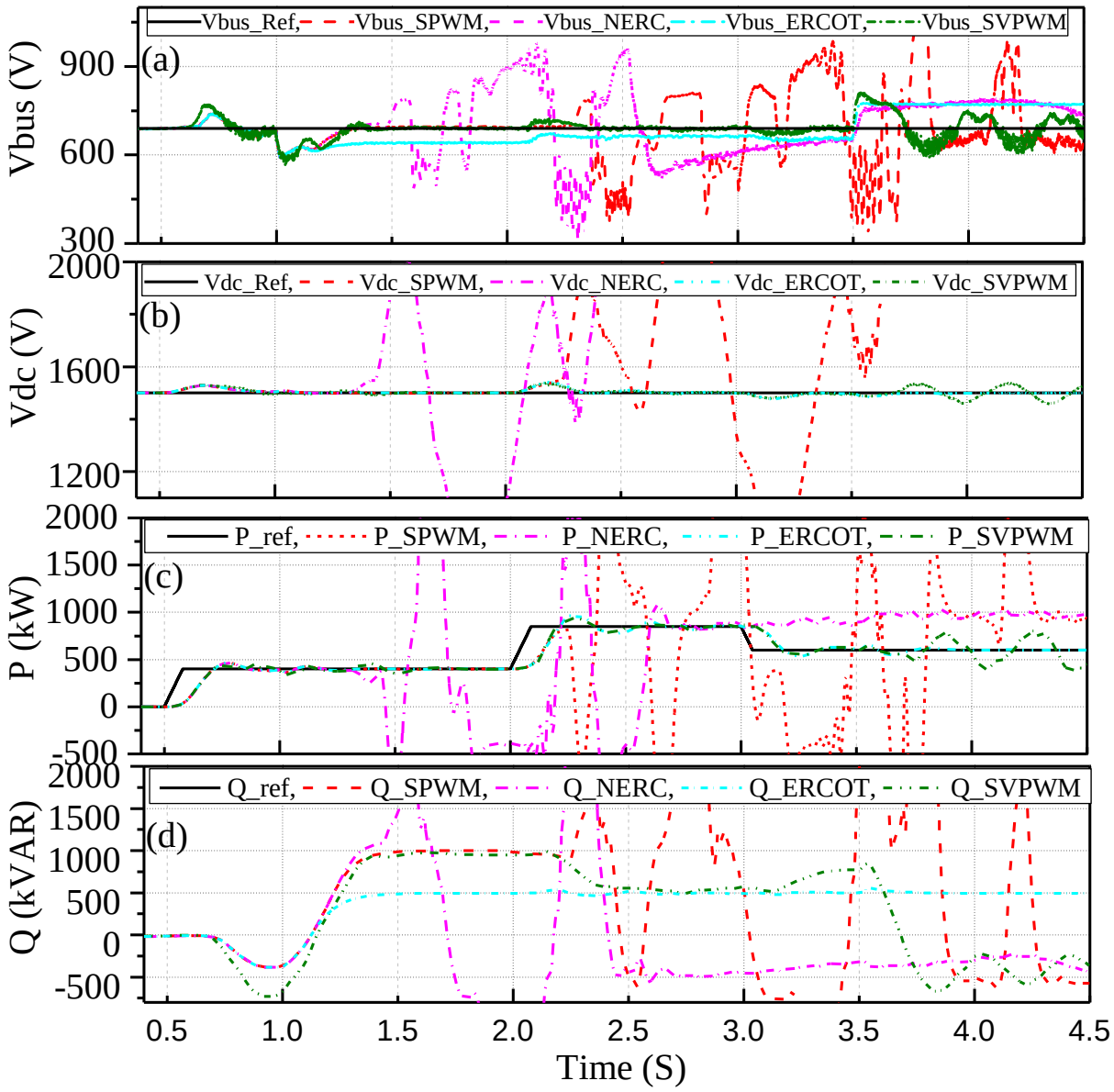

Fig. 7.11. IBR operation under a varying grid impedance condition: a) *PCC* bus voltage (RMS), b) *dc*-link voltage, c) active power to the grid at the *PCC*, d) reactive power to the grid at the *PCC*

8. CONCLUSION

IBR P-Q capability is an important factor for the power industry to assure the safe operation of an IBR and for the power and energy community to develop international IBR standards as well. This thesis presents a comprehensive P-Q capability evaluation for IBRs with different filtering mechanisms and PWM strategies. The study carefully considers specific IBR characteristics as well as the specific nature of IBR control in the dq reference frame. The results show that IBR P-Q capability chart is quite different from that of a synchronous generator and from the traditional IBR P-Q capability charts used in the industry. The study indicates that design of an IBR, such as selections of dc-link voltage and filter inductance, is important to assure IBR P-Q capability curve that can meet the grid interconnection requirements. The study also shows that the variations of real-time parameters and grid conditions could affect the actual physical IBR P-Q capability chart a lot and significantly shrink the permissible P-Q capability, which certainly would affect the safe operation of IBRs. The study shows that the dynamic nature of IBR P-Q capability could cause an abnormal operation of an IBR at both strong and weak grid conditions and affect IBR low and high voltage ride through capability. Furthermore, the study shows the derivation of IBR P-Q capability curve with a L-filter equation, which can help industry use by different working condition, and the method to explore more area of the IBR technology such as IBR capability in LC and LCL filter, or IBR capability on type 3 wind turbine. As a result, development of new IBR control technology that can guarantee efficient and

reliable operation of IBRs at any grid conditions is urgently needed. For the future, there will be continues research on the IBR P-Q capability curve for the Doubly-Fed induction generator.

REFERENCES

[1] REN21, "Global Status Report 2016," available at http://www.ren21.net/wp-content/uploads/2016/06/GSR_2016_FullReport.pdf.

[2] N.E. Nilsson, and J. Mercurio, "Synchronous generator capability curve testing and evaluation," IEEE Trans. Power Del., 9(1), pp.414-424, 1994.

[3] M.M. Adibi, and D.P. Milanicz, "Reactive capability limitation of synchronous machines," IEEE Trans. Power Syst., 9(1), pp.29-40, 1994.

[4] University of Wisconsin-Madison, "Estimating Generator Capability Curves," available at https://neos-guide.org/sites/default/files/capability_curves.pdf.

[5] IEEE Standard for Interconnection and Interoperability of Distributed Energy Resources with Associated Electric Power Systems Interfaces," in IEEE Std 1547-2018 (Revision of IEEE Std 1547-2003), vol., no., pp.1-138, 6 April 2018.

[6] P2800 - Standard for Interconnection and Interoperability of Inverter-Based Resources Interconnecting with Associated Transmission Electric Power Systems, Project Details at https://standards.ieee.org/project/2800.html.

[7] North American Electric Reliability Corporation, "Reliability Guideline BPS-Connected Inverter-Based Resource Performance," Sep. 2018, available at https://www.nerc.com/comm/OC_Reliability_Guidelines_DL/Inverter-Based_Resource_Performance_Guideline.pdf.[8] ERCOT, "Inverter-Based Resource (IBR) Workshop," available at http://ercot.com/content/wcm/key_documents_lists/176763/ERCOT_IBR_Workshop_April_25_2019.pdf.

[9] A. Ellis, R. Nelson, E.V. Engeln, R. Walling, J. McDowell, L. Casey, E. Seymour, W. Peter, C. Barker, and B. Kirby, "Reactive Power Interconnection Requirements for PV and Wind Plants," SANDIA REPORT - SAND2012-1098, Sandia National Laboratories, Feb. 2012.

[10] R.N. Beres, X. Wang, M. Liserre, F. Blaabjerg, and C.L. Bak, "A review of passive power filters for three-phase grid-connected voltage-source converters," IEEE J. Emerg. Sel. Topics Power Electron., 4(1), pp.54-69, 2015.

[11] C. Li, "Unstable Operation of Photovoltaic Inverter From Field Experiences," IEEE Trans. Power Del, vol. 33, no. 2, pp. 1013-1015, April 2018.

[12] C. Li, "On Capacitor Switching Transient Immunity of Inverter-Based Renewable Generations," IEEE Trans. Power Del, vol. 30, no. 5, pp. 2339-2345, Oct. 2015.

[13] IEEE Technical Report on Impact of Inverter Based Resources on Utility Transmission System Protection, prepared by Power System Relay and Control Committee Subcommittee C – System Protection Working Group C32, Jan. 2019.

[14] A. Adib, B. Mirafzal, X. Wang and F. Blaabjerg, "On Stability of Voltage Source Inverters in Weak Grids," IEEE Access, vol. 6, pp. 4427-4439, 2018.

[15] Xu, J., Xie, S. and Tang, T., "Evaluations of current control in weak grid case for grid-connected LCL-filtered inverter," IET Power Electronics, 6(2), pp.227-234,. 2013.

[16] Chen, X., Zhang, Y., Wang, S., Chen, J. and Gong, C., "Impedance-phased dynamic control method for grid-connected inverters in a weak grid," IEEE Trans. Power Electron., 32(1), pp.274-283, 2016.

[17] Xie, B., Guo, K., Mao, M., Zhou, L., Liu, T., Zhang, Q. and Hao, G., "Analysis and Improved Design of Phase Compensated Proportional Resonant Controllers for Grid-Connected Inverters in Weak Grid," IEEE Trans. Energy Convers., 2020.

[18] Z. Chen, J. M. Guerrero, and F. Blaabjerg, “A review of the state of the art of power electronics for wind turbines,” IEEE Trans. Power Electron., vol. 24, no. 8, pp. 1859–1875, Aug. 2009.

[19] B.K. Santhoshi, K.M. Sundaram, S. Padmanaban, J.B. Holm-Nielsen, and K.K. Prabhakaran, "Critical Review of PV Grid-Tied Inverters," Energies 2019, 12(10), 1921; https://doi.org/10.3390/en12101921.

[20] B. Xie, Y. Liu, Y. Ji, and J. Wang, "Two-stage battery energy storage system (BESS) in AC microgrids with balanced state-of-charge and guaranteed small-signal stability," Energies, 11(2), p.322, 2018.

[21] N. Mohan, T. M. Undeland, and W. P. Robbins, Power Electronics: Converters, Applications, and Design, 3rd Ed., John Wiley & Sons Inc., Oct. 2002.

[22] N. Mohan, Advanced Electric Drives – Analysis, Modeling and Control using MATLAB/Simulink, John Wiley & Sons, ISBN 978-1-118-48548-4, 2014.

[23] S. Li, T. Haskew, and L. Xu, “Conventional and Novel Control Designs for Direct Driven PMSG Wind Turbines,” Electric Power System Research (Elsevier), Vol. 80, Issue 3, March 2010, pp. 328-338.

[24] K. Zhou and D. Wang, "Relationship between space-vector modulation and three-phase carrier-based PWM: a comprehensive analysis," IEEE Trans. Ind. Electron., 49(1), (2002): 186-196.

[25] R. Peña-Alzola et al., “Analysis of the passive damping losses in LCL filter-based grid converters,” IEEE Trans. Power Electron., vol. 28, no. 6, pp. 2642–2646, Jun. 2013.

[26] R. Gagnon and J. Brochu, "Wind Farm - Synchronous Generator and Full Scale Converter (Type 4) Detailed Model," The MathWork, Jan. 2019

[27] M. Liserre, A. Dell'Aquila and F. Blaabjerg, "Design and control of a three-phase active rectifier under non-ideal operating conditions," *Conference Record of the 2002 IEEE Industry Applications Conference. 37th IAS Annual Meeting.* Pittsburgh, PA, USA, 2002, pp. 1181-1188

[28] F. Blaabjerg, F. Iov, R. Teodorescu and Z. Chen, "Power Electronics in Renewable Energy Systems," *2006 12th International Power Electronics and Motion Control Conference*, Portoroz, 2006, pp. 1-17.

[29] G. Wang et al., "A Review of Power Electronics for Grid Connection of Utility-Scale Battery Energy Storage Systems," in IEEE Transactions on Sustainable Energy, vol. 7, no. 4, pp. 1778-1790, Oct. 2016, doi: 10.1109/TSTE.2016.2586941.